"Ra'di", Younes; Simovski, Constantin R.; Tretyakov, Sergei A.

Thin perfect absorbers for electromagnetic waves: Theory, design, and realizations

Published in:
Physical Review Applied

DOI:
10.1103/PhysRevApplied.3.037001

Published: 01/01/2015

Document Version
Publisher's PDF, also known as Version of record

PHYSICAL REVIEW APPLIED 3, 037001 (2015)

Thin Perfect Absorbers for Electromagnetic Waves: Theory, Design, and Realizations

Y. Ra'di,* C. R. Simovski, and S. A. Tretyakov

Department of Radio Science and Engineering, School of Electrical Engineering, Aalto University, P.O. Box 13000, FI-00076 Aalto, Finland

(Received 24 October 2014; published 17 March 2015)

With recent advances in nanophotonics and nanofabrication, considerable progress has been achieved in realizations of thin composite layers designed for full absorption of incident electromagnetic radiation, from microwaves to the visible. If the layer is structured at a subwavelength scale, thin perfect absorbers are usually called "metamaterial absorbers," because these composite structures are designed to emulate some material responses not reachable with any natural material. On the other hand, many thin absorbing composite layers were designed and used already in the time of the introduction of radar technology, predominantly as a means to reduce radar visibility of targets. In view of a wide variety of classical and new topologies of optically thin metamaterial absorbers and plurality of applications, there is a need for a general, conceptual overview of the fundamental mechanisms of full absorption of light or microwave radiation in thin layers. Here, we present such an overview in the form of a general theory of thin perfectly absorbing layers. Possible topologies of perfect metamaterial absorbers are classified based on their fundamental operational principles. For each of the identified classes, we provide design equations and give examples of particular realizations. The concluding section provides a summary and gives an outlook on future developments in this field.

DOI: 10.1103/PhysRevApplied.3.037001

I. INTRODUCTION

In numerous applications of electromagnetic waves, from radio to optical frequencies, there is a need to design and realize layers which effectively absorb the power of incident electromagnetic waves. Dallenbach [1] and Salisbury [2] absorbers are classical examples of microwave absorbers, developed along the work on the first radars. The Dallenbach absorber uses a lossy dielectric layer backed by a metal ground plane. The layer thickness is close to a quarter wavelength in the dielectric, so that the input impedance is real. The loss tangent of the dielectric is chosen so that the input resistance is matched with the free-space impedance. The thickness of Salisbury screens is also equal to a quarter wavelength: A single resistive sheet is located at quarter-wavelength distance from the metal ground, where the electric field resulting from the interference of the incident and mirror-reflected waves has the maximum value. Information on classical microwave absorbers based on the use of conventional and artificial materials can be found in Refs. [3–5]. Analysis of singe- and multilayered Salisbury absorbers can be found in Ref. [6]. Because of their resonant sizes, most of these absorbers are considerably thick. The absorption frequency band of optically thick absorbers can be quite wide, but the considerable thickness of these structures makes them not practical for many applications. To absorb visible light, layers of various black substances have been used from prehistorical times. Also, in this case the absorbers are very thick in terms of the wavelength. Naturally, there is a need for electrically thin structures (in radio-engineering language, it means the same as optically thin, i.e., much thinner than the wavelength) as microwave absorbers. At present, the research focus is on optically thin terahertz and optical absorbers. This research is motivated by the current development of nanotechnologies and new arising applications in optical [7] and terahertz [8] sensing of individual quantum objects and energy harvesting for solar-photovoltaic [9] and thermophotovoltaic [10] systems. These new applications require the perfect absorption of a certain spectrum of incident light in submicron layers. The recent literature has witnessed great activity in designing thin absorbers for infrared and optical frequencies. Figure 1 illustrates typical topologies of nearly perfect absorbers for microwave, terahertz, and infrared frequencies. Interestingly, all of these devices are similar in what concerns the operational principle (Sec. V B 4).

As we shall see, there are many possibilities to realize full absorption of normally incident plane waves in extremely thin layers, but perfect absorption takes place at just one frequency (or possibly at a set of discrete frequencies). For thin absorbers, the most practically relevant problem is the fundamental limitation on the absorption bandwidth for absorbers of a given thickness [15,16]. Another important issue is the sensitivity of absorption on the incidence angle and polarization of the incident waves. Considerable work has been done in

*Corresponding author.
younes.radi@aalto.fi

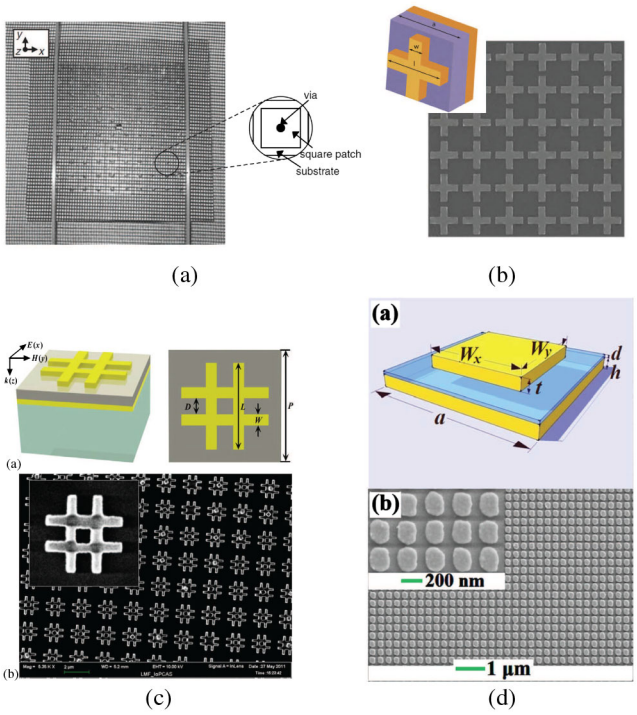

FIG. 1. (a) Experimental realizations of thin nearly perfect absorbers at microwaves. This figure is reproduced with permission [11]. ©The Institution of Engineering and Technology. (b) Experimental realizations of thin nearly perfect absorbers at terahertz. This figure is reproduced with permission [12]. ©SPIE publication. (c) Experimental realizations of thin nearly perfect absorbers at infrared [13]. ©IOP Publishing. This figure is reproduced by permission of IOP Publishing. All rights reserved. (d) Experimental realizations of thin nearly perfect absorbers at near-infrared frequencies. This figure is reprinted with permission from Ref. [14]. Copyright (2010), AIP Publishing LLC.

finding designs providing angular- and polarization-stable operation of thin absorbers (see, e.g., Refs. [13,17–25]).

In many recent papers, the name *perfect absorber* is adopted for a structure which has zero-reflection and transmission coefficients for normally incident plane waves at one given frequency. This terminology appears unfortunate, because from the engineering point of view a perfect absorber would work at all frequencies and for all incident angles and polarizations. Moreover, the same word perfect already appears in the name of the perfectly matched layer [26], which is indeed perfect in the sense that it fully absorbs waves of any polarization coming from any direction. Of course, perfect absorbers in the engineering sense do not exist. In traditional terminology, a boundary which fully absorbs a normally incident plane wave at one frequency is called the *matched boundary*. However, since the term perfect absorber appears to be commonly accepted in the current literature, we use it also in this review.

In a sense, the design of perfect absorbers (stressing again, perfect at one frequency and for one incidence angle only) is rather trivial. Just like a load characterized by an arbitrary impedance with a nonzero real part can be matched to a cable with any characteristic impedance using only one reactive element, any reflector-backed material layer of any nonzero thickness (except totally lossless layers) can be forced to fully absorb normally incident plane waves at one frequency using only one reactive frequency-selective surface (the frequency-selective surface is a sheet characterized by some reactive averaged surface impedance, for example, an array of thin metal patches [4]). However, if we impose conditions on the allowed thickness and materials, and, most importantly, on the absorption bandwidth and angular stability, design tasks will be far from trivial and simple.

Recently, the work on perfect absorbers has been focused on the use of metamaterials and metasurfaces, two-dimensional analogues of metamaterials. Probably the first known realization of thin metamaterial absorbers is based on the use of artificial impedance surfaces [27]. On a surface with a very high reactive surface impedance, the magnetic field is close to zero and the electric field equals twice the incident electric field. Positioning a resistive sheet at such a high-impedance surface (HIS), one can effectively dissipate the incident power and decrease reflectivity to zero. Later, it was shown that there is no need for a separate resistive sheet, and full absorption in high-impedance structures can be realized by using a lossy dielectric as a substrate [19]. Another implementation of the same idea is the use of an array of split-ring resonators (SRRs) to realize an artificial magnetic conductor and position a resistive sheet on top of that surface [28]. More recently, after the publication of Ref. [29], where the name *metamaterial-based perfect absorber* is introduced, designs of thin composite absorbing layers (now commonly called *metamaterial-based absorbers*) developed earlier for microwave frequencies have been extended to higher frequencies, up to the visible range. There have been perfect absorbers reported in terahertz [12,30], near-infrared [31], and visible light [23] frequencies. A recent review of metamaterial-based electromagnetic wave absorbers can be found in Ref. [32]. These absorbers can be potentially used in filters and sensors, for solar energy harvesting, and for many other applications [7,9,25,33–45].

For the design and optimization of these structures, it is really critical to understand the physical phenomena which ensure the absorber operation. One needs conceptually simple and clear models which should give the conditions on the effective parameters of the composite layers as targets for the design and optimization. Earlier approaches are based on the description of thin absorbing layers as effectively homogeneous bulk media or on using the methods based on impedance matching [29,46–49]. The main idea in this approach is to tune the effective permittivity ϵ and permeability μ of a metamaterial absorber to match the effective wave impedance of the absorber $\eta = \sqrt{\mu/\epsilon}$ to the free-space wave impedance

$\eta_0 = \sqrt{\mu_0/\epsilon_0}$. However, the use of this method is limited by the problem of the applicability of the effective medium model to (usually single) arrays of resonant cells. There are also methods based on the reflection interference model [50–53]. Another popular method is using circuit- and transmission-line-based models [54–59]. Also, models and explanations based on Fabry-Pérot and other cavity resonances [60–62] have been introduced as alternative interpretations of the absorption mechanism in metamaterial absorbers.

Although all these models explain the same physical phenomena, they are not always ideal in clarifying different physical aspects of the processes in various absorbers and for use as design tools. In some of these models interactions between inclusions in the absorbing array are not taken into account, and in some others near-field interactions between two layers on the two sides of a spacer are neglected. The majority of the known models are mostly qualitative and cannot be used as effective design tools, so that the design is based only on extensive numerical simulations and optimizations. Moreover, the analysis of recent literature shows that there is still some confusion in the explanations of the absorption mechanisms. For example, in Refs. [51,63], it is claimed that a magnetic response is not necessary to realize metamaterial-based absorbers. However, opposite statements are found in numerous publications, e.g., Refs. [46,64–66]. Another physically important aspect of the perfect absorption in thin layers is the symmetry or asymmetry of absorption for illumination of the two opposite sides of the absorbing structure. In fact, the possible asymmetry of absorption is linked to bianisotropic properties of the layers (excitation of both electric and magnetic polarizations by both electric and magnetic excitations), and it is possible to find very general and simple design requirements for all kinds of electrically thin perfect absorbers, both symmetric and asymmetric at illuminations from the opposite sides [67].

The goal of this tutorial overview is to provide a general view on the phenomenon of perfect absorption in optically thin layers, give the most general design equations for the required induced currents, and provide classification of perfect absorbers based on their operational principles. Explanations of the general concepts are complemented by a broad overview of particular realizations of perfect absorbers of each fundamental class, which illustrate and exemplify the general design principles. The concluding section summarizes the state of the art and provides an outlook for further developments.

II. PERFECT ABSORBERS: OPERATIONAL PRINCIPLE

Here we will show that the operational principles of any thin perfect absorber can be well understood in terms of effective electric- and magnetic-current sheets which model the polarization and conduction currents induced in the respective composite structures. Figure 2 illustrates a generic composite layer illuminated by a normally incident plane wave. The layer thickness is assumed to be optically small, so that the layer can be considered as a *metasurface:* a microscopically structured sheet (usually periodic) with the period of the structure smaller than the wavelength in the surrounding media. This restriction on the period is necessary to ensure that the absorbing layer does not generate diffraction lobes, and for an observer in the far zone the response is that of an effectively homogeneous sheet. We do not impose any other restrictions on the geometry of the layer. It can be asymmetric with respect to the two sides; it can be asymmetric with respect to mirror inversion (chiral) or have nonreciprocal elements (magnetized ferrite or plasma inclusions).

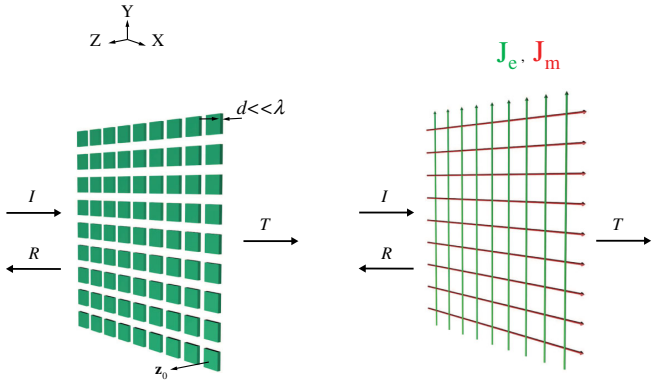

FIG. 2. Geometry of a generic optically thin absorbing layer (left) and its equivalent model as a set of two current sheets (right).

Under the assumption of an electrically small thickness and the period smaller than the wavelength, the reflected and transmitted waves are plane waves created by the surface-averaged electric- and magnetic-current sheets $\mathbf{J}_e$ and $\mathbf{J}_m$, respectively, as illustrated in Fig. 2. In composite sheets, the layer has a complicated microstructure, usually containing some electrically small but resonant inclusions (such as complex-shape patches or split rings or small helices). The surface-averaged current densities can be related to the electric and magnetic dipole moments $\mathbf{p}$ and $\mathbf{m}$, respectively, induced in each unit cell as

$$\mathbf{J}_e = \frac{j\omega\mathbf{p}}{S}, \qquad \mathbf{J}_m = \frac{j\omega\mathbf{m}}{S}. \tag{1}$$

Here S is the unit-cell area, and we use the time-harmonic convention $\exp(j\omega t)$. The higher-order multipoles induced in the unit cells do not contribute to the radiated plane-wave fields of the infinite array (higher-order modes are important in calculations of the dependence of the induced averaged currents on the incident fields).

In this overview, we describe thin composite layers acting as perfect absorbers, that is, layers which have zero-reflection and transmission coefficients: $R = T = 0$. We formulate the necessary requirements on the induced

surface-current densities and explain how these requirements can be realized in various absorbing structures.

A. General considerations

To ensure zero reflection and zero transmission, the absorber device must create a forward-directed plane wave which cancels the incident plane wave. At the same time, the absorber device should not create any radiation in the direction towards the source (no reflection). First of all, we note that an infinitely thin sheet of any nonmagnetic material cannot act as a perfect absorber. It is clear from the fact that, in this case, conduction or polarization currents induced on the sheet by the incident plane wave are confined to one plane in space. This current sheet will radiate symmetrically in the forward and backward directions, while a perfect absorber should radiate only in the forward direction. In fact, it is easy to show that an infinitely thin sheet can absorb maximum 50% of the incident power (e.g., Ref. [68]). This simple consideration brings us to a conclusion that any perfect absorber must have a nonzero physical thickness (the use of negligibly thin magnetic-material sheets implies nonphysical infinite values of the permeability).

The simplest volumetric distribution of current in a thin finite-thickness layer is a set of two parallel infinitely thin sheets of electric current. Thus, let us next consider an absorber device formed by two parallel material or composite sheets separated by distance d. The incident field will induce some electric currents on the two sheets (conduction or displacement currents), and we denote the corresponding surface-current densities as $\mathbf{J}_{e1}$ and $\mathbf{J}_{e2}$. Let the incident plane wave come from the side of sheet 1, and its amplitude at the position of the second sheet is $\mathbf{E}_{\text{inc}}$. The two sheets will act as a perfect absorber if the sum of the electric fields in two plane waves created by the two sheets cancels the incident field behind the second sheet:

$$-\frac{\eta_0}{2}\mathbf{J}_{e1}e^{-jk_0d}-\frac{\eta_0}{2}\mathbf{J}_{e2}=-\mathbf{E}_{\text{inc}}, \tag{2}$$

while the electric fields of the two reflected plane waves cancel in the opposite direction:

$$-\frac{\eta_0}{2}\mathbf{J}_{e1}-\frac{\eta_0}{2}\mathbf{J}_{e2}e^{-jk_0d}=\mathbf{0}. \tag{3}$$

Here, η_0 is the free-space impedance and k_0 is the propagation constant. The above formulas for the amplitudes of electric fields created by electric-current sheets simply express the classical boundary conditions on surfaces which maintain surface currents [a more general form valid for oblique incidence can be found, e.g., in Eq. (4.34) of Ref. [69]]. The solution of this system of equations reads

$$\mathbf{J}_{e1}=\frac{j}{\eta_0\sin(k_0d)}\mathbf{E}_{\text{inc}}, \tag{4}$$

$$\mathbf{J}_{e2}=-\frac{je^{jk_0d}}{\eta_0\sin(k_0d)}\mathbf{E}_{\text{inc}}. \tag{5}$$

In this simple case of currents concentrated on two sheets, we have a unique solution for the surface-current densities of a perfect absorber (for a fixed thickness d). Examples of absorbers of this type include the Salisbury screen [2] and lossy capacitive grids (for example, arrays of patches) over a ground plane [11,19,27], which we will call *high-impedance surface absorbers*. While the realizations can be quite different, in all of these absorbers the surface-current densities on the two layers obey (4) and (5).

Let us next find the required boundary conditions on the two surfaces, relating the electric surface-current densities with the total tangential fields on these surfaces. Actually, Eq. (2) implies that in absorbers formed by only two electric-current sheets the second surface must be perfectly electrically conducting (PEC boundary). Indeed, Eq. (2) directly states that the total tangential electric field at the second surface

$$\mathbf{E}_{\text{tot}}=\mathbf{E}_{\text{inc}}-\frac{\eta_0}{2}\mathbf{J}_{e1}e^{-jk_0d}-\frac{\eta_0}{2}\mathbf{J}_{e2}=\mathbf{0}. \tag{6}$$

As a check, one can use the last relation to express the incident field in terms of the total field and current densities and substitute in Eq. (5). As a result, it is seen that the surface impedance of the second surface is zero ($\mathbf{J}_{e2}\times 0=\mathbf{E}_{\text{tot}}$). Because also the tangential magnetic field behind a perfect absorber is zero, the theory can be reformulated for the dual case of a perfect magnetic conductor (PMC) as a second surface or, more generally, for an arbitrary boundary. From the practical point of view, this result tells us that within this realization scenario we need at least three effective current sheets to realize symmetric absorbers (equally absorbing from both sides).

Of course, the boundary condition Eq. (6) bounds only the surface-averaged fields and currents, which means that the conclusion that the second sheet is a PEC or PMC boundary holds only for homogeneous-material sheets. In structured layers, the evanescent fields formed close to the inhomogeneities do not equal zero everywhere at and behind the second sheet (they exponentially decay behind and in front of the absorber). We will see examples of absorbers formed by arrays of particles without any ground plane in the following sections.

Let us write the required sheet impedance of the first sheet, which relates the total electric field and the surface-current density $\mathbf{J}_{e1}$ at that plane. The total field is the sum of the incident field $\mathbf{E}_{\text{inc}}e^{jk_0d}$ at that plane and the fields created by electric currents $\mathbf{J}_{e1,2}$ induced on the two surfaces, but, since the reflection coefficient is zero, the sum of the fields created by the currents is zero [Eq. (3)]. Thus, we can write the total field at the first sheet as

$$\mathbf{E}_{\rm tot} = \mathbf{E}_{\rm inc} e^{jk_0 d} = Z_g \mathbf{J}_{e1} = -j\eta_0 \sin(k_0 d) e^{jk_0 d} \mathbf{J}_{e1}. \quad (7)$$

Here we have expressed $\mathbf{E}_{\rm inc}$ in terms of $\mathbf{J}_{e1}$ using Eq. (4). We see that the required sheet (grid) impedance [69] of the first layer reads

$$Z_g = -j\eta_0 \sin(k_0 d) e^{jk_0 d}, \quad (8)$$

and the corresponding admittance equals

$$Y_g = \frac{1}{Z_g} = \frac{j}{\eta_0} \frac{e^{-jk_0 d}}{\sin(k_0 d)} = \frac{j}{\eta_0 \tan k_0 d} + \frac{1}{\eta_0}. \quad (9)$$

As an example, for the Salisbury absorber ($d = \lambda_0/4$, $k_0 d = \pi/2$), Eq. (8) shows that the surface impedance of the first layer should be purely resistive and equal to $Z_g = \eta_0$. In the modern optical literature, the effect of full absorption in a thin sheet when the matching condition Eq. (9) is satisfied is usually called *critical coupling* [70–74]. Because of the complexity of actual geometries used in optical devices, the effect is usually revealed by using numerical optimizations. However, the physics of this effect is the same as of the Salisbury absorber described in Ref. [75]. If the distance between the two sheets is arbitrary (usually considerably smaller than $\lambda_0/4$), Eqs. (8) and (9) give the general design requirements for high-impedance surface absorbers [see Eq. (90), discussions in Sec. V B 4, and detailed derivations in Appendix A].

More generally, we can consider perfect absorbers where induced currents are filling the whole volume of a slab of the thickness d instead of being concentrated only on two sheets. In this case, the requirements for perfect absorption take the form of two integral equations [the sums in Eqs. (2) and (3) replaced by integrals over the slab thickness], and the solution for the required current densities is no longer unique.

An important conclusion at this stage is that for perfect absorption of the power of a plane wave we need to ensure that the absorber creates at least two coherent and interfering plane waves, to enable asymmetric actions in the forward and backward directions. These waves can be created by current sheets induced on two infinitesimally thin layers (one of them can be a mirror), by currents in the whole volume of a slab, or by other means. With this respect, it is interesting to note recent papers on so-called "coherent absorbers," where the second coherent wave is created by splitting the incident beam into two and directing both beams to the same thin lossy sheet via a system of mirrors [76–79] or a prism [80]. The name coherent absorber was introduced in Ref. [81] as specific to that particular device, but, as we see, the operation of any perfect absorber is based on interference of mutually coherent waves. Actually, in any perfect absorber where the energy is dissipated in an optically thin layer, that layer is illuminated by two (or more) coherent plane waves. The operational principle of the two-beam device [76] is very similar to the Salisbury screen [2] or the circuit-analog absorber [4], where the second incident coherent beam, which illuminates a thin absorbing sheet, is created simply by a mirror behind a lossy sheet.

Let us note in passing that Eqs. (4) and (5) suggest a possibility to realize an active absorber if the incident field is known. Indeed, if we know $\mathbf{E}_{\rm inc}$ in advance, we can realize the required surface-current densities by constructing, for example, two arrays of electric dipole antennas fed by appropriately chosen sources. Although the system is active, for the incident plane wave it will work as a perfect absorber. This idea is similar to the recently introduced concept of the active cloak [82,83], where arrays of antennas are used to generate fields which cancel fields scattered from an object which one wants to cloak.

After this brief discussion which concerns resonant perfect absorbers of any thickness, let us next consider the fundamentals of optically thin absorbing layers.

B. Optically thin perfect absorbers

The operational principle of a generic optically thin absorber is convenient to explain by using the same example of two polarizable sheets tuned to work as a perfect absorber. Let us rewrite Eqs. (2) and (3) in terms of the symmetric and antisymmetric surface-current sheets, defining

$$\mathbf{J}_s = \frac{1}{2}(\mathbf{J}_{e1} + \mathbf{J}_{e2}), \qquad \mathbf{J}_a = \frac{1}{2}(\mathbf{J}_{e2} - \mathbf{J}_{e1}). \quad (10)$$

Equations (2) and (3) take the form

$$-\frac{\eta_0}{2}\mathbf{J}_s(1 + e^{-jk_0 d}) - \frac{\eta_0}{2}\mathbf{J}_a(1 - e^{-jk_0 d}) = -\mathbf{E}_{\rm inc}, \quad (11)$$

$$-\frac{\eta_0}{2}\mathbf{J}_s(1 + e^{-jk_0 d}) - \frac{\eta_0}{2}\mathbf{J}_a(-1 + e^{-jk_0 d}) = 0. \quad (12)$$

For optically thin (meaning that $|k_0|d \ll 1$) absorbers, we can replace the exponents with the first terms of their Taylor expansions. The first term in Eqs. (11) and (12) reduces to

$$-\frac{\eta_0}{2}\mathbf{J}_s(1 + e^{-jk_0 d}) \approx -\frac{\eta_0}{2}(2\mathbf{J}_s) = -\frac{\eta_0}{2}(\mathbf{J}_{e1} + \mathbf{J}_{e2}). \quad (13)$$

We recognize this quantity as the electric field of the plane wave generated by the electric-current sheet

$$\mathbf{J}_e = \mathbf{J}_{e1} + \mathbf{J}_{e2} \quad (14)$$

at the position of this sheet. Obviously, the surface-current density $\mathbf{J}_e$ is simply the total electric-current density induced in the thin absorber.

The second term in Eq. (11) for thin absorbers simplifies to

$$-\frac{\eta_0}{2}\mathbf{J}_a(1-e^{-jk_0d}) \approx -\frac{\eta_0}{2}\mathbf{J}_a jk_0 d = -\frac{1}{2}(j\omega\mu_0 d)\mathbf{J}_a. \tag{15}$$

We recognize this quantity as the electric field of the plane wave generated by a sheet of magnetic current at the absorber plane. Indeed, the magnetic surface-current density $\mathbf{J}_m$ is related to the magnetic moment per unit area $\mathbf{M}$ as $\mathbf{J}_m = j\omega\mathbf{M}$, and the magnetic moment is related to the antisymmetric part of the electric-current distribution as $\mathbf{M} = -\mu_0 d\mathbf{z}_0 \times \mathbf{J}_a$ ($\mathbf{z}_0$ is the unit vector normal to the absorber plane and pointing towards the source of the incident plane wave). Thus, $j\omega\mu_0 d\mathbf{J}_a = \mathbf{z}_0 \times \mathbf{J}_m$.

Finally, Eqs. (11) and (12) take the physically clear, simple, and general form

$$-\frac{\eta_0}{2}\mathbf{J}_e - \frac{1}{2}\mathbf{z}_0 \times \mathbf{J}_m = -\mathbf{E}_{\text{inc}}, \tag{16}$$

$$-\frac{\eta_0}{2}\mathbf{J}_e + \frac{1}{2}\mathbf{z}_0 \times \mathbf{J}_m = \mathbf{0}. \tag{17}$$

Solving these equations, we find the required electric and magnetic surface-current densities:

$$\mathbf{J}_e = \frac{1}{\eta_0}\mathbf{E}_{\text{inc}}, \tag{18}$$

$$\mathbf{z}_0 \times \mathbf{J}_m = \mathbf{E}_{\text{inc}}, \qquad \mathbf{J}_m = -\mathbf{z}_0 \times \mathbf{E}_{\text{inc}} = \eta_0\mathbf{H}_{\text{inc}}. \tag{19}$$

As a check, we can see that the same follows directly from Eqs. (4) and (5) in the assumption $k_0 d \ll 1$:

$$\mathbf{J}_e = \mathbf{J}_{e1} + \mathbf{J}_{e2} = \frac{1}{\eta_0}\frac{j}{k_0 d}(1-e^{jk_0 d})\mathbf{E}_{\text{inc}} \approx \frac{1}{\eta_0}\mathbf{E}_{\text{inc}}, \tag{20}$$

$$\mathbf{J}_m = -j\omega\mu_0\frac{d}{2}\mathbf{z}_0 \times (\mathbf{J}_{e2} - \mathbf{J}_{e1}) \approx -\omega\mu_0\frac{d}{2}\frac{2}{\eta_0 k_0 d}\mathbf{z}_0 \times \mathbf{E}_{\text{inc}} = -\mathbf{z}_0 \times \mathbf{E}_{\text{inc}} = \eta_0\mathbf{H}_{\text{inc}}. \tag{21}$$

Although we have derived these formulas considering a model of two polarizable sheets, it is clear that the result in fact holds for any optically thin absorber, because the plane-wave response of any optically thin structure reduces to plane-wave fields created by surface-averaged electric- and magnetic-current sheets, as illustrated in Fig. 2. We can use this result for thin homogeneous layers, periodical structures, and arrays of discontinuous cells, with the only limitation that the structural period in the absorber plane is smaller than the wavelength in free space (ensuring that no diffracted plane waves are generated). For absorbers realized in the form of arrays of particles (or any disconnected unit cells), it is more convenient to rewrite Eqs. (16) and (17) in terms of the electric ($\mathbf{p}$) and magnetic ($\mathbf{m}$) dipole moment of a single unit cell. As already discussed, these dipole moments relate to the respective surface-current densities as in Eq. (1).

C. Thin absorbers as Huygens sheets

Two important conclusions follow from Eqs. (16) and (17). First of all, and as was already noted before, a thin perfect absorber must support both electric and magnetic surface currents (both $\mathbf{J}_e$ and $\mathbf{J}_m$ must be nonzero). Indeed, if one of them is zero, then the other one must be also zero to ensure zero reflection, and in that case the layer is fully transparent. Second, we observe that any optically thin perfect absorber is a Huygens surface, because the induced surface-current densities obey the relation (17):

$$\eta_0\mathbf{J}_e = \mathbf{z}_0 \times \mathbf{J}_m, \tag{22}$$

which is the same as the relation between the electric and magnetic fields in the incident plane wave. Physically, this result means that the plane-wave fields created by the induced electric and magnetic currents cancel each other in the backward direction (again we see interference of two mutually coherent plane waves). Let us stress also here that this conclusion holds for any optically thin layer which has a zero-reflection coefficient. In the case of a perfect absorber, the two waves sum up in the forward direction and cancel the incident field [Eq. (16)].

Actual realizations can contain some homogeneous layers (e.g., a thin slab of magnetic or dielectric material on a PEC ground plane) or periodical arrays with the transverse period smaller than the wavelength in free space (e.g., arrays of resonant dielectric spheres, double arrays of metal patches, or arrays of metal patches over a PEC plane). In the case of a periodical structure, it can be more convenient to write the equations in terms of electric and magnetic dipole moments induced in each unit cell, $\mathbf{p}$ and $\mathbf{m}$; then Eq. (22) takes the form

$$\eta_0\mathbf{p} = \mathbf{z}_0 \times \mathbf{m}. \tag{23}$$

Because the dipole moments of cells and the surface-averaged current densities are simply proportional to each other [Eq. (1)], both continuous and periodical absorbers can be understood in terms of induced electric and magnetic moments, either per unit cell or per unit area.

III. THIN PERFECT ABSORBERS: GENERAL DESIGN EQUATIONS

In the previous section, we found the required values of induced surface-current densities which ensure perfect absorption of a normally incident plane wave. Next, we address the design question: What should be the electromagnetic parameters of the layer, such that the induced currents indeed take the desired values? As discussed above, the electromagnetic response of thin material or composite sheets can be described in terms of either

relations for induced surface-current densities or induced electric and magnetic moments per unit cell or per unit area. We will first use the formalism of induced dipole moments. The material of this section is based on Ref. [67].

A. Induced polarization densities and currents

In the most general case of a thin linear sheet, composite or homogeneous, we can write the linear relations between the induced moments in each unit cell (or in a unit area of the sheet) and the incident fields as

$$\begin{bmatrix} \mathbf{p} \\ \mathbf{m} \end{bmatrix} = \begin{bmatrix} \bar{\bar{\hat{\alpha}}}_{ee} & \bar{\bar{\hat{\alpha}}}_{em} \\ \bar{\bar{\hat{\alpha}}}_{me} & \bar{\bar{\hat{\alpha}}}_{mm} \end{bmatrix} \cdot \begin{bmatrix} \mathbf{E}_{\text{inc}} \\ \mathbf{H}_{\text{inc}} \end{bmatrix}. \tag{24}$$

Here the dual bars denote dyadic (tensor) quantities, and the hat marks the collective polarizabilities, which measure the response of the unit cells to external fields incident on the infinite array. For composite sheets, these polarizabilities include the effects of particle interactions and depend not only on the individual cell topology and dimensions but also on the distances to the other inclusions in the lattice. In view of Eq. (1), this dependence is equivalent to relating the induced surface-current densities to the incident fields. Indeed, Eq. (24) is equivalent to

$$\begin{bmatrix} \mathbf{J}_e \\ \mathbf{J}_m \end{bmatrix} = \frac{j\omega}{S} \begin{bmatrix} \bar{\bar{\hat{\alpha}}}_{ee} & \bar{\bar{\hat{\alpha}}}_{em} \\ \bar{\bar{\hat{\alpha}}}_{me} & \bar{\bar{\hat{\alpha}}}_{mm} \end{bmatrix} \cdot \begin{bmatrix} \mathbf{E}_{\text{inc}} \\ \mathbf{H}_{\text{inc}} \end{bmatrix} \tag{25}$$

(S is the unit-cell area). We know that in perfect absorbers the induced current densities relate to the incident fields as in Eqs. (18) and (19). Thus, we can determine the required unit-cell polarizabilities of perfect absorbers as solutions of the following system of equations:

$$\frac{j\omega}{S} \begin{bmatrix} \bar{\bar{\hat{\alpha}}}_{ee} & \bar{\bar{\hat{\alpha}}}_{em} \\ \bar{\bar{\hat{\alpha}}}_{me} & \bar{\bar{\hat{\alpha}}}_{mm} \end{bmatrix} = \begin{bmatrix} \frac{1}{\eta_0}\bar{\bar{I}}_t & 0 \\ 0 & \eta_0 \bar{\bar{I}}_t \end{bmatrix}. \tag{26}$$

Here, $\bar{\bar{I}}_t$ is the two-dimensional unit dyadic (matrix) defined in the absorber plane. Obviously, there are infinitely many solutions for the polarizabilities, since we have more free design parameters than the number of equations. To clarify the possible choices and different absorption and matching mechanisms, it is more convenient to first find the reflection and transmission coefficients in terms of the collective polarizabilities and then study what combinations of these parameters realize perfect absorbers.

To do that, first we note that the dyadics in Eqs. (24) and (26) are not the most general two-dimensional dyadics, but they possess rotational symmetry, because perfect absorbers should absorb normally incident plane waves of any polarization. This property means that the absorber structure should have no preferred direction along the absorber plane. In terms of the electromagnetic parameters, the layer must be a uniaxial structure, where the only preferred direction is given by the unit vector normal to the surface, $\mathbf{z}_0$. The uniaxial symmetry ensures the isotropic response for normally incident plane waves of arbitrary polarizations.

Thus, for the most general thin perfect absorber we can write all the polarizabilities in (24) in the form

$$\begin{aligned} \bar{\bar{\hat{\alpha}}}_{ee} &= \hat{\alpha}_{ee}^{\text{co}}\bar{\bar{I}}_t + \hat{\alpha}_{ee}^{\text{cr}}\bar{\bar{J}}_t, \qquad \bar{\bar{\hat{\alpha}}}_{mm} = \hat{\alpha}_{mm}^{\text{co}}\bar{\bar{I}}_t + \hat{\alpha}_{mm}^{\text{cr}}\bar{\bar{J}}_t, \\ \bar{\bar{\hat{\alpha}}}_{em} &= \hat{\alpha}_{em}^{\text{co}}\bar{\bar{I}}_t + \hat{\alpha}_{em}^{\text{cr}}\bar{\bar{J}}_t, \qquad \bar{\bar{\hat{\alpha}}}_{me} = \hat{\alpha}_{me}^{\text{co}}\bar{\bar{I}}_t + \hat{\alpha}_{me}^{\text{cr}}\bar{\bar{J}}_t, \end{aligned} \tag{27}$$

where indices co and cr refer to the symmetric and antisymmetric parts of the corresponding dyadics, respectively. Here, $\bar{\bar{I}}_t = \bar{\bar{I}} - \mathbf{z}_0\mathbf{z}_0$ is the two-dimensional unit dyadic, and $\bar{\bar{J}}_t = \mathbf{z}_0 \times \bar{\bar{I}}_t$ is the vector-product operator. In the last set of relations, it is convenient to separate the coupling coefficients responsible for reciprocal and nonreciprocal coupling processes:

$$\begin{aligned} \bar{\bar{\hat{\alpha}}}_{em} &= (\hat{\chi} + j\hat{\kappa})\bar{\bar{I}}_t + (\hat{V} + j\hat{\Omega})\bar{\bar{J}}_t, \\ \bar{\bar{\hat{\alpha}}}_{me} &= (\hat{\chi} - j\hat{\kappa})\bar{\bar{I}}_t + (-\hat{V} + j\hat{\Omega})\bar{\bar{J}}_t. \end{aligned} \tag{28}$$

In the following, we use the classification of magnetoelectric coupling effects in terms of reciprocity and the symmetry of their magnetoelectric coupling dyadics. There are two reciprocal classes (chiral and omega, measured by the parameters $\hat{\kappa}$ and $\hat{\Omega}$, respectively) and two nonreciprocal classes ("moving" and Tellegen, measured by $\hat{V}$ and $\hat{\chi}$, respectively) [5]. The four main types of magnetoelectric coupling are summarized in Table I. Note also that for reciprocal particles the electric and magnetic polarizabilities $\bar{\bar{\hat{\alpha}}}_{ee}$ and $\bar{\bar{\hat{\alpha}}}_{mm}$ are always symmetric dyadics; that is, $\hat{\alpha}_{ee}^{\text{cr}} = 0$ and $\hat{\alpha}_{mm}^{\text{cr}} = 0$ in all reciprocal structures.

In the rest of the review, we use double signs to distinguish the illuminations of the thin absorbing layer from its two sides, where the top and bottom signs correspond to the incident plane wave propagating along the $-\mathbf{z}_0$ and $\mathbf{z}_0$ directions, respectively (Fig. 2). In the incident plane wave, the electric and magnetic fields satisfy

$$\mathbf{H}_{\text{inc}} = \mp \frac{1}{\eta_0}\mathbf{z}_0 \times \mathbf{E}_{\text{inc}}. \tag{29}$$

Radiation from infinite sheets of electric and magnetic currents can be easily solved (e.g., Ref. [84]), and the electric field amplitudes in the reflected ($\mathbf{E}_{\text{ref}}$) and transmitted ($\mathbf{E}_{\text{tr}}$) plane waves are written as

$$\begin{aligned} \mathbf{E}_{\text{ref}} &= -\frac{j\omega}{2S}[\eta_0\mathbf{p} \mp \mathbf{z}_0 \times \mathbf{m}], \\ \mathbf{E}_{\text{tr}} &= \mathbf{E}_{\text{inc}} - \frac{j\omega}{2S}[\eta_0\mathbf{p} \pm \mathbf{z}_0 \times \mathbf{m}]. \end{aligned} \tag{30}$$

TABLE I. Magnetoelectric coupling effects (parameters Ω, κ, V, and χ for lossless structures are real).

Omega	Chiral	Moving	Tellegen
$\bar{\bar{\alpha}}_{em} = \bar{\bar{\alpha}}_{me} = j\Omega\bar{\bar{J}}_t$	$\bar{\bar{\alpha}}_{em} = -\bar{\bar{\alpha}}_{me} = j\kappa\bar{\bar{I}}_t$	$\bar{\bar{\alpha}}_{em} = -\bar{\bar{\alpha}}_{me} = V\bar{\bar{J}}_t$	$\bar{\bar{\alpha}}_{em} = \bar{\bar{\alpha}}_{me} = \chi\bar{\bar{I}}_t$

Expressing the induced dipole moments in terms of the incident electric field and the polarizabilities in the form of Eq. (28), we get

$$\mathbf{E}_{\rm ref} = -\frac{j\omega}{2S}\left\{\left[\eta_0\hat{\alpha}_{ee}^{\rm co} \pm 2j\hat{\Omega} - \frac{1}{\eta_0}\hat{\alpha}_{mm}^{\rm co}\right]\bar{\bar{I}}_t + \left[\eta_0\hat{\alpha}_{ee}^{\rm cr} \mp 2\hat{\chi} - \frac{1}{\eta_0}\hat{\alpha}_{mm}^{\rm cr}\right]\bar{\bar{J}}_t\right\}\cdot\mathbf{E}_{\rm inc}, \tag{31}$$

$$\mathbf{E}_{\rm tr} = \left\{\left[1 - \frac{j\omega}{2S}\left(\eta_0\hat{\alpha}_{ee}^{\rm co} \pm 2\hat{V} + \frac{1}{\eta_0}\hat{\alpha}_{mm}^{\rm co}\right)\right]\bar{\bar{I}}_t - \frac{j\omega}{2S}\left[\eta_0\hat{\alpha}_{ee}^{\rm cr} \mp 2j\hat{\kappa} + \frac{1}{\eta_0}\hat{\alpha}_{mm}^{\rm cr}\right]\bar{\bar{J}}_t\right\}\cdot\mathbf{E}_{\rm inc}. \tag{32}$$

General expressions (31) and (32) for the reflected and transmitted fields from planar uniaxial bianisotropic layers allow the derivation of required conditions for perfect absorption in terms of the polarizabilities of the unit cells. By definition, a perfect absorber does not reflect power and creates perfect shadow behind the sheet; that is,

$$\mathbf{E}_{\rm ref} = \mathbf{0}, \qquad \mathbf{E}_{\rm tr} = \mathbf{0}. \tag{33}$$

Let us consider the two requirements of perfect absorption Eq. (33) separately.

B. Zero-reflection condition for collective polarizabilities

As discussed above, the zero-reflection property requires that the layer behaves as a Huygens sheet, with the induced dipole moments satisfying Eq. (23). From Eq. (31), we see that the zero-reflection condition requires the following relation between the two polarizabilities (electric and magnetic) and the omega coupling coefficient:

$$\eta_0\hat{\alpha}_{ee}^{\rm co} \pm 2j\hat{\Omega} - \frac{1}{\eta_0}\hat{\alpha}_{mm}^{\rm co} = 0 \tag{34}$$

(under this condition the copolarized reflection vanishes). Let us recall that the $\pm$ signs in this relation refer to illuminations from the two sides of the thin layer. Thus, if there is no magnetoelectric coupling in the layer ($\hat{\Omega} = 0$), the reflection coefficient is the same for illumination from both sides. In particular, it is clear that any thin absorber on a metal surface is a bianisotropic layer with omega coupling in the microstructure. This result is obvious from the fact that the reflection coefficient from the side of the ground plane is always -1, while it is zero from the side of the absorbing layer.

Continuing the analysis of the zero-reflection requirement, we note that the cross-polarized reflection vanishes if

$$\eta_0\hat{\alpha}_{ee}^{\rm cr} \mp 2\hat{\chi} - \frac{1}{\eta_0}\hat{\alpha}_{mm}^{\rm cr} = 0. \tag{35}$$

All the polarizabilities which enter this relation can have nonzero values only if the layer is nonreciprocal. In view of practical realizations, the simplest way to ensure that Eq. (35) is valid is to use only reciprocal materials in the absorber design. If nonreciprocity is required (for example, to realize different transmission coefficients for waves coming from the opposite directions), the nonreciprocal responses due to electric, magnetic, and magnetoelectric polarization processes must be balanced as is dictated by Eq. (35) in order to ensure zero reflection from the absorber. In the following, we concentrate on reciprocal absorbers. Nonreciprocal absorbing sheets are discussed in Ref. [67].

C. Zero transmission condition for collective polarizabilities

The transmitted field is zero when the sum of the plane-wave fields created by induced electric- and magnetic-current sheets compensates the incident field:

$$\frac{j\omega}{2S}[\eta_0\mathbf{p} \pm \mathbf{z}_0 \times \mathbf{m}] = \mathbf{E}_{\rm inc}. \tag{36}$$

Recall that the amplitudes of waves created by the electric and magnetic dipole moments are equal (as they cancel out in the reflected field). Again, we note that magnetoelectric coupling (nonreciprocal parameter $\hat{V}$) is responsible for the possible difference of transmission coefficients for illumination from the two sides of the sheet. Naturally, for reciprocal sheets ($\hat{V} = 0$) the transmission coefficient is the same as seen from both sides, and the requirement of full absorption reads

$$\eta_0\hat{\alpha}_{ee}^{\rm co} + \frac{1}{\eta_0}\hat{\alpha}_{mm}^{\rm co} = \frac{2S}{j\omega}. \tag{37}$$

If the sheet is reciprocal, then the electric and magnetic polarizabilities are symmetric dyadics ($\hat{\alpha}_{ee}^{\rm cr} = 0$, $\hat{\alpha}_{mm}^{\rm cr} = 0$), which brings us to the conclusion that all reciprocal polarization-insensitive thin perfect absorbers are nonchiral ($\hat{\kappa} = 0$). With this respect, we note that this conclusion does

not exclude the use of chiral elements (like metal spirals) in the design of thin absorbers. However, for proper operation, chiral elements should be arranged so that the overall structure of the layer is nonchiral. The most common known topologies contain random mixtures or regular arrays of chiral particles over a perfectly conducting ground plane [85–87]. Because the mirror images of spirals have the opposite handedness, the overall response is nonchiral (the reflected wave has the same polarization as the incident wave, if the arrangement of spirals is isotropic, and the transmitted field is zero behind the PEC plane). A discussion about advantages of microscopically chiral absorbers can be found in Ref. [87] and references therein.

In summary, thin perfect reciprocal absorbers which absorb waves incident on both sides of the sheet are simple electrically and magnetically polarizable layers (no bianisotropy). Thin perfect reciprocal absorbers which absorb waves incident only on one side of the sheet (various reflection properties are possible if one illuminates the other side) are bianisotropic layers with the antisymmetric coupling dyadic (omega structures). Equations (34) and (37) give the necessary conditions on the collective polarizabilities of the unit cells of perfect absorbers.

D. Required values of collective polarizabilities

For the most general case of thin reciprocal perfect absorbers, we can assume that the response can be asymmetric, meaning that only one side of the layer is perfectly absorbing, while the other side is characterized by the reflection coefficient R. From Eqs. (31) and (32), we find the requirements on the collective polarizabilities in terms of the reflection coefficient R of the "imperfect" side:

$$\eta_0\hat{\alpha}_{ee}^{\mathrm{co}} + 2j\hat{\Omega} - \frac{1}{\eta_0}\hat{\alpha}_{mm}^{\mathrm{co}} = 0, \tag{38}$$

$$-\frac{j\omega}{2S}\left(\eta_0\hat{\alpha}_{ee}^{\mathrm{co}} - 2j\hat{\Omega} - \frac{1}{\eta_0}\hat{\alpha}_{mm}^{\mathrm{co}}\right) = R, \tag{39}$$

$$\eta_0\hat{\alpha}_{ee}^{\mathrm{co}} + \frac{1}{\eta_0}\hat{\alpha}_{mm}^{\mathrm{co}} = \frac{2S}{j\omega}. \tag{40}$$

Solving for the required polarizabilities, we find

$$\eta_0\hat{\alpha}_{ee}^{\mathrm{co}} = \left(1 - \frac{R}{2}\right)\frac{S}{j\omega}, \tag{41}$$

$$j\hat{\Omega} = \frac{R}{2}\frac{S}{j\omega}, \tag{42}$$

and

$$\frac{1}{\eta_0}\hat{\alpha}_{mm}^{\mathrm{co}} = \left(1 + \frac{R}{2}\right)\frac{S}{j\omega}. \tag{43}$$

Let us write the induced electric and magnetic currents for a sheet with such polarizabilities. Suppose that the perfectly absorbing side is illuminated (the incident wave propagates along $-\mathbf{z}_0$). In this bianisotropic layer, the electric current is induced by both the electric and magnetic fields:

$$\mathbf{J}_e = \frac{j\omega}{S}\mathbf{p} = \frac{j\omega}{S}(\hat{\alpha}_{ee}^{\mathrm{co}}\mathbf{E}_{\mathrm{inc}} + j\hat{\Omega}\mathbf{z}_0 \times \mathbf{H}_{\mathrm{inc}}). \tag{44}$$

Using the plane-wave relation between the fields in the incident wave, $\mathbf{z}_0 \times \mathbf{H}_{\mathrm{inc}} = \mathbf{E}_{\mathrm{inc}}/\eta_0$, and substituting the parameters from Eqs. (41) and (42), we find that

$$\mathbf{J}_e = \frac{j\omega}{S}\left(\hat{\alpha}_{ee}^{\mathrm{co}} + \frac{1}{\eta_0}j\hat{\Omega}\right)\mathbf{E}_{\mathrm{inc}} = \frac{1}{\eta_0}\mathbf{E}_{\mathrm{inc}}, \tag{45}$$

for an arbitrary reflection coefficient R of the opposite side of the layer. Thus, the necessary relation between the incident field and induced current Eq. (18) is indeed satisfied. Similarly, one can check that the induced magnetic current satisfies Eq. (19) for any R.

Let us specialize the above results for the case when a thin absorbing structure is covering a perfectly conducting surface (the most interesting scenario for microwave absorbers). In this situation, the reflection coefficient from the PEC side equals -1, while we demand perfect absorption in the cover. If the structure is perfectly absorbing plane waves traveling along $-\mathbf{z}_0$ and fully reflects ($R = -1$) waves propagating along $\mathbf{z}_0$, the polarizabilities read

$$\eta_0\hat{\alpha}_{ee}^{\mathrm{co}} = \frac{3}{2}\frac{S}{j\omega}, \tag{46}$$

$$j\hat{\Omega} = -\frac{1}{2}\frac{S}{j\omega}, \tag{47}$$

and

$$\frac{1}{\eta_0}\hat{\alpha}_{mm}^{\mathrm{co}} = \frac{1}{2}\frac{S}{j\omega}. \tag{48}$$

It is important to note that, due to the omega coupling, the induced electric and magnetic surface-current densities are balanced, although the normalized magnetic polarizability is 3 times as small as the electric polarizability. From the point of view of realizations at very high frequencies (especially in the infrared and visible ranges), the main problem is to provide enough strong magnetic response, because naturally magnetic media are not available, and artificial magnetism is a weak second-order effect of spatial dispersion (e.g., Ref. [5]). The possibility to use stronger, first-order effects of bianisotropic omega coupling is clearly an advantageous route. If it is enough to ensure full absorption only from one side of the layer and the

reflection coefficient from the other side can be arbitrary, it is reasonable to choose the realization with the smallest possible absolute value of the required magnetic polarizability $\hat{\alpha}^{\rm co}_{mm}$. Inspecting Eq. (43), we see that the best choice is the case of full mirror reflection from the back side, $R=-1$.

To realize symmetric perfect absorption from both sides of a thin layer, we must ensure that

$$\eta_0\hat{\alpha}^{\rm co}_{ee}=\frac{1}{\eta_0}\hat{\alpha}^{\rm co}_{mm}=\frac{S}{j\omega}. \tag{49}$$

In this case there is no magnetoelectric coupling, and the electric and magnetic responses are balanced (equally strong).

It is important to note that the results of this section are not restricted by any assumption on the explicit topology of bianisotropic sheets. The structure can contain one or several composite or homogeneous layers, and the required conditions for induced electric and magnetic polarizations may be realized in structures which mimic the required bianisotropic response, not containing any bianisotropic particles with dipolar response.

IV. REQUIRED SURFACE SUSCEPTIBILITIES AND UNIT-CELL POLARIZABILITIES

A. Symmetric absorbers: Impedance or admittance boundary conditions

While the above relations for the required induced electric- and magnetic-current densities and collective polarizabilities of unit cells provide good insight into the operational principle of perfect absorbers, for the design of absorbing layers it is more convenient to express the current densities as functions of the *total* tangential electric and magnetic fields, so that the coefficients would have the usual meaning of surface impedance or admittance. For symmetric structures (both sides perfectly absorptive), we can find the total surface-averaged fields right on the absorbing sheet plane as the averaged values of the tangential fields on the two opposite surfaces of the layer:

$$\mathbf{E}_{\rm tot}=\frac{1}{2}(\mathbf{E}_{+}+\mathbf{E}_{-}),\qquad \mathbf{H}_{\rm tot}=\frac{1}{2}(\mathbf{H}_{+}+\mathbf{H}_{-}). \tag{50}$$

The total fields can be related to the induced surface-current densities simply by noticing that the total fields on the surface are the sums of the incident fields and the fields created by the currents on the surface:

$$\mathbf{E}_{\rm tot}=\mathbf{E}_{\rm inc}-\frac{\eta_0}{2}\mathbf{J}_e, \tag{51}$$

$$\mathbf{H}_{\rm tot}=\mathbf{H}_{\rm inc}-\frac{1}{2\eta_0}\mathbf{J}_m. \tag{52}$$

Note that, with the current values given by Eqs. (18) and (21), relations (50) are equivalent to

$$\mathbf{E}_{\rm tot}=\frac{1}{2}\mathbf{E}_{\rm inc},\qquad \mathbf{H}_{\rm tot}=\frac{1}{2}\mathbf{H}_{\rm inc} \tag{53}$$

(this is expected, because on the illuminated side the field equals to the incident field, and on the other side it is zero). Substituting the incident fields into Eqs. (18) and (19), we find that on the surface of a symmetric perfectly absorbing sheet the following sheet conditions are satisfied:

$$\mathbf{J}_e=\frac{2}{\eta_0}\mathbf{E}_{\rm tot},\qquad \mathbf{J}_m=2\eta_0\mathbf{H}_{\rm tot}. \tag{54}$$

Thus, the layer is a set of two purely resistive (the coefficients in the above relations are purely real) sheets: one electric, with the surface resistance equal to $\eta_0/2$, and the dual "magnetic resistor" sheet, both positioned at the same plane of the sheet absorber.

B. Asymmetric absorbers

1. Impedance or admittance matrices

For asymmetric absorbers, the impedance or admittance matrix (e.g., Ref. [69]) is an appropriate model. In this model, the structure response is described in terms of linear relations between the total fields at the two sides of the layer:

$$\begin{pmatrix}\mathbf{E}_{+}\\ \mathbf{E}_{-}\end{pmatrix}=\begin{pmatrix}Z_{11} & Z_{12}\\ Z_{21} & Z_{22}\end{pmatrix}\cdot\begin{pmatrix}\mathbf{z}_0\times\mathbf{H}_{+}\\ \mathbf{z}_0\times\mathbf{H}_{-}\end{pmatrix}. \tag{55}$$

Here the indices $\pm$ mark the tangential fields at the two opposite sides of the layer. Let us find the impedance parameters for a layer acting as a perfect absorber from the "+" side (incident waves along the $-\mathbf{z}_0$ direction) and having reflection coefficient R for the illumination of the opposite side (the same as considered in Sec. III D). To do that, we write the expression (55) first for illuminations of the absorbing side and then for the reflecting side:

$$\begin{pmatrix}\mathbf{E}_{\rm inc}\\ 0\end{pmatrix}=\begin{pmatrix}Z_{11} & Z_{12}\\ Z_{21} & Z_{22}\end{pmatrix}\cdot\begin{pmatrix}\mathbf{z}_0\times\mathbf{H}_{\rm inc}\\ 0\end{pmatrix}, \tag{56}$$

$$\begin{pmatrix}0\\ (1+R)\mathbf{E}_{\rm inc}\end{pmatrix}=\begin{pmatrix}Z_{11} & Z_{12}\\ Z_{21} & Z_{22}\end{pmatrix}\cdot\begin{pmatrix}0\\ -(1-R)\mathbf{z}_0\times\mathbf{H}_{\rm inc}\end{pmatrix}. \tag{57}$$

Obviously, these relations are satisfied if

$$Z_{11}=\eta_0,\qquad Z_{22}=-\eta_0\frac{1+R}{1-R},\qquad Z_{12}=Z_{21}=0. \tag{58}$$

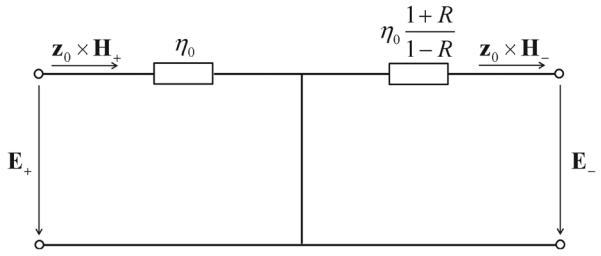

FIG. 3. T-circuit model of a perfectly absorbing layer.

Knowing the Z matrix, we can find the parameters of the equivalent T circuit (e.g., Sec. 2.4 in Ref. [69]). The result is shown in Fig. 3. Obviously, the symmetric absorber which is modeled as a set of resistive sheets in the same plane [Eq. (54)] corresponds to a symmetric T circuit with both impedances equal to η_0.

Similarly, to determine the structure of the equivalent Π circuit, we can find the parameters of the admittance matrix $\bar{\bar{Y}}$:

$$\begin{pmatrix}\mathbf{z}_0\times\mathbf{H}_+\\ \mathbf{z}_0\times\mathbf{H}_-\end{pmatrix}=\begin{pmatrix}Y_{11} & Y_{12}\\ Y_{21} & Y_{22}\end{pmatrix}\cdot\begin{pmatrix}\mathbf{E}_+\\ \mathbf{E}_-\end{pmatrix}, \tag{59}$$

which is the inverse of $\bar{\bar{Z}}$. Its components read

$$Y_{11}=\frac{1}{\eta_0},\qquad Y_{22}=-\frac{1}{\eta_0}\frac{1-R}{1+R},\qquad Y_{12}=Y_{21}=0. \tag{60}$$

This matrix corresponds to the equivalent Π circuit shown in Fig. 4. For the purposes of the topology design, it may be convenient to make use of the equivalent scattering or transmission matrices of the layer. They can be found by using standard formulas of microwave engineering, e.g., Ref. [88].

The presence of either short- or open-circuit components in the equivalent networks does not imply that the actual realizations of perfect absorbers must include an impenetrable wall. In fact, these two equivalent T and Π circuits can model one and the same absorber, which does not contain neither electric nor magnetic wall. For symmetric absorbers ($R=0$ in the above relations), the equivalent circuits are symmetric and contain only resistors equal to η_0. Such absorbers can be modeled both as a symmetric two-port, described in terms of matrix $\bar{\bar{Z}}$ or $\bar{\bar{Y}}$, or as a set of two resistive sheets (one electric and one magnetic, in the same plane), described by relations (54). If the absorber is asymmetric ($R\neq 0$), the two-port matrix model (55) is appropriate. The relations between the asymmetry of the equivalent circuit and the omega-type bianisotropy of the physical structure are analyzed in detail in Ref. [89].

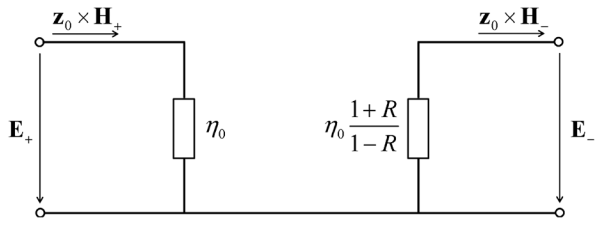

FIG. 4. Π-circuit model of a perfectly absorbing layer (the shown values are resistances).

2. Required parameters of discrete unit cells (individual polarizabilities)

In the previous section, we derived the required effective parameters of asymmetric perfect absorbers in terms of their impedance or admittance matrices. However, there is a useful alternative model for asymmetric perfect absorbers which consist of an array of electrically small particles. If the interaction of particles in the array can be considered as the interaction of corresponding electric and magnetic dipoles, it is possible to find the required polarizabilities of a single individual particle in free space, such that, when arranged in a lattice, a perfect absorber would be realized. Knowing the requirements on single particles allows designing individual unit cells.

Finding relations between collective and individual polarizabilities is one of the fundamental problems of applied electromagnetics, and it has been discussed in dozens of papers and (for simple dipole arrays) in books, e.g., Ref. [69]. For understanding and designing perfect absorbers, we need a rather general solution presenting the relation between the collective and individual polarizabilities in closed form which would be applicable beyond the quasistatic approximation (which is used in most publications). Moreover, here we need the solution for bianisotropic arrays. Recently, in Ref. [67], the needed expressions were found for uniaxial square arrays of bianisotropic particles whose electric and magnetic moments are induced in the array plane. By using these results, for arrays of bianisotropic omega particles the individual polarizabilities as functions of the collective ones can be written as

$$\begin{aligned}\alpha_{ee}^{\mathrm{co}}&=\frac{\hat{\alpha}_{ee}^{\mathrm{co}}+\beta_m(\hat{\alpha}_{ee}^{\mathrm{co}}\hat{\alpha}_{mm}^{\mathrm{co}}-\hat{\Omega}^2)}{1+(\beta_e\hat{\alpha}_{ee}^{\mathrm{co}}+\beta_m\hat{\alpha}_{mm}^{\mathrm{co}})+\beta_e\beta_m(\hat{\alpha}_{ee}^{\mathrm{co}}\hat{\alpha}_{mm}^{\mathrm{co}}-\hat{\Omega}^2)},\\ \alpha_{mm}^{\mathrm{co}}&=\frac{\hat{\alpha}_{mm}^{\mathrm{co}}+\beta_e(\hat{\alpha}_{ee}^{\mathrm{co}}\hat{\alpha}_{mm}^{\mathrm{co}}-\hat{\Omega}^2)}{1+(\beta_e\hat{\alpha}_{ee}^{\mathrm{co}}+\beta_m\hat{\alpha}_{mm}^{\mathrm{co}})+\beta_e\beta_m(\hat{\alpha}_{ee}^{\mathrm{co}}\hat{\alpha}_{mm}^{\mathrm{co}}-\hat{\Omega}^2)},\\ \Omega&=\frac{\hat{\Omega}}{1+(\beta_e\hat{\alpha}_{ee}^{\mathrm{co}}+\beta_m\hat{\alpha}_{mm}^{\mathrm{co}})+\beta_e\beta_m(\hat{\alpha}_{ee}^{\mathrm{co}}\hat{\alpha}_{mm}^{\mathrm{co}}-\hat{\Omega}^2)}.\end{aligned} \tag{61}$$

Explicit analytical expressions for the interaction constants β_e and β_m can be found, e.g., in Ref. [69]. As an example, let us give explicit design formulas for an asymmetric absorber which is fully reflective ($R=-1$) from the nonabsorbing side. The required collective polarizabilities are given by Eqs. (46)–(48). Substituting into the above relations, we find that the required individual polarizabilities of unit cells read

$$\alpha_{ee}^{\mathrm{co}}=\frac{\frac{3}{2}+\frac{\beta_e}{j\omega\eta_0}}{(1+\frac{\beta_e}{j\omega\eta_0})^2}\frac{1}{j\omega\eta_0},$$
$$\alpha_{mm}^{\mathrm{co}}=\frac{\frac{1}{2}+\frac{\beta_e}{j\omega\eta_0}}{(1+\frac{\beta_e}{j\omega\eta_0})^2}\frac{\eta_0}{j\omega},$$
$$\Omega=\frac{\frac{1}{2}}{(1+\frac{\beta_e}{j\omega\eta_0})^2}\frac{1}{\omega}. \tag{62}$$

By knowing these required polarizabilities of one single unit cell in free space, the shape and dimensions of the particle can be found from analytical models or by using numerical simulation and optimization techniques.

V. POSSIBLE REALIZATIONS OF PERFECTLY ABSORBING SHEETS

Next, we consider particular realizations of thin absorbers and explain how they realize the required conditions on induced electric- and magnetic-current sheets to form absorptive Huygens pairs. We start from the simpler case of symmetric structures, equally absorbing power from both sides of the layer.

A. Symmetric perfect absorbers

1. Impedance-matched layers

Let us consider a material layer with $\mu_r=\epsilon_r$. Because the impedance is equal to that of free space, at an interface with such a medium there is no reflection (considering only normal incidence). If we in addition assume that the material is very lossy, the wave will quickly decay, and we can use an electrically thin (compared to the free-space wavelength) layer as a perfect absorber. In practice, one can position this layer on a PEC ground plane, if the thickness d is such that the wave decays before reaching the PEC plane. It is possible if $k_0 d|\sqrt{\epsilon_r\mu_r}|\gg 1$.

To find the equivalent electric surface-current density in the skin layer, we first write the volumetric-current density

$$\mathbf{j}_e=j\omega\mathbf{P}=j\omega(\mathbf{D}-\epsilon_0\mathbf{E})=j\omega\epsilon_0(\epsilon_r-1)\mathbf{E}, \tag{63}$$

where $\mathbf{E}$ is the electric field inside the absorbing layer. The electric field at the input interface equals the incident field (because there is no reflected wave), and in the layer it exponentially decays: $\mathbf{E}(z)=\mathbf{E}_{\mathrm{inc}}e^{-jk_0\sqrt{\epsilon_r\mu_r}z}$. The equivalent surface-current density is found as an integral of the volumetric-current density over the skin depth:

$$\mathbf{J}_e=\int_0^\infty \mathbf{j}_e dz=j\omega\epsilon_0(\epsilon_r-1)\frac{1}{jk_0\sqrt{\epsilon_r\mu_r}}\mathbf{E}_{\mathrm{inc}}\approx\frac{1}{\eta_0}\mathbf{E}_{\mathrm{inc}}, \tag{64}$$

in the assumption $|\epsilon_r|=|\mu_r|\gg 1$. Because of duality, we can do the same derivation for the magnetic current to obtain

$$\mathbf{J}_m=\int_0^\infty \mathbf{j}_m dz=j\omega\mu_0(\mu_r-1)\frac{1}{jk_0\sqrt{\epsilon_r\mu_r}}\mathbf{H}_{\mathrm{inc}}\approx\eta_0\mathbf{H}_{\mathrm{inc}}. \tag{65}$$

As we see, the induced surface current densities are indeed the same as required for perfect absorption in a thin sheet [Eqs. (20) and (21)].

Now we can find the effective impedances and admittances, relating the induced surface current densities to the total tangential electric and magnetic fields in the sheet plane, instead of the incident fields as in Eqs. (64) and (65). To do that, we add to the left- and right-hand sides of Eq. (64) the plane-wave fields created by $\mathbf{J}_e$ (the electric fields generated by $\mathbf{J}_m$ differ by sign on the two sides of the sheet and, thus, do not contribute to the averaged electric field):

$$\eta_0\mathbf{J}_e-\frac{\eta_0}{2}\mathbf{J}_e=\mathbf{E}_{\mathrm{inc}}-\frac{\eta_0}{2}\mathbf{J}_e=\mathbf{E}_{\mathrm{tot}}. \tag{66}$$

Thus,

$$\mathbf{J}_e=\frac{2}{\eta_0}\mathbf{E}_{\mathrm{tot}}. \tag{67}$$

Likewise, we obtain

$$\mathbf{J}_m=2\eta_0\mathbf{H}_{\mathrm{tot}}. \tag{68}$$

As expected, these are the required resistive-sheet conditions for symmetric absorbers (54). In this case, the magnetoelectric coupling is absent, because essentially we assume that the wave decays to zero over the slab thickness. The same isotropic slab can be illuminated from the opposite direction, and the power will be equally totally absorbed. As we have shown before, in this case thin absorbers have no bianisotropy. Practical realizations of sheets implementing the condition $k_0 d|\sqrt{\epsilon_r\mu_r}|\gg 1$ with $\mu_r=\epsilon_r$ are challenging due to the lack of materials with the needed permittivity and permeability, especially for broadband and high-frequency applications.

2. Arrays of small resonant particles

The required electromagnetic properties of matched absorbing layers can be emulated by periodical arrays of small resonant particles. The electromagnetic properties of dense arrays (the period is smaller than the wavelength in the surrounding medium) can be modeled by the grid impedance Z_g, which connects the averaged electric surface-current density $\mathbf{J}_e$ and the averaged tangential electric field in the array plane:

$$\mathbf{E}_{\text{tot}} = Z_g \mathbf{J}_e. \tag{69}$$

For perfect absorption, the required value of this parameter is $Z_g = \eta_0/2$ [Eq. (54)]. In terms of the polarizability of each individual particle in the array, the grid impedance reads [69]

$$Z_g = -j\frac{S}{\omega}\left[\text{Re}\left(\frac{1}{\alpha_{ee}} - \beta_e\right) + j\left(\text{Im}\frac{1}{\alpha_{ee}} - \frac{k_0^3}{6\pi\epsilon_0}\right)\right]. \tag{70}$$

Here, α_{ee} is the electric polarizability of one inclusion in free space, β_e is the interaction constant in the infinite array, and, as before, S is the unit-cell area. Apparently, in order to achieve perfect absorption, the imaginary part of Z_g should vanish. Physically, this requirement means that we should work at the resonance frequency of the particles in the array [the reactive coupling with the other inclusions is modeled by $\text{Re}(\beta_e)$]. Equating the real part of the grid impedance to $\eta_0/2$, we find the required loss parameter of the inclusions. Obviously, the imaginary part of the inverse polarizability should satisfy

$$\text{Im}\left(\frac{1}{\alpha_{ee}}\right) = \frac{\eta_0}{2}\frac{\omega}{S} + \frac{k_0^3}{6\pi\epsilon_0}. \tag{71}$$

The last term (proportional to k_0^3) is the measure of scattering loss of any dipole particle, and the first term tells how strong dissipation we need in each particle. Note that the required absorption parameter is inversely proportional to the unit-cell area S. This result means that there is no need to tune the particle losses to a prescribed value, as the overall losses can be adjusted varying the array period. Dual relations hold for the magnetic-current density and magnetic fields, from which we find the required condition on magnetic losses in each particle:

$$\text{Im}\left(\frac{1}{\alpha_{mm}}\right) = \frac{1}{2\eta_0}\frac{\omega}{S} + \frac{k_0^3}{6\pi\mu_0}. \tag{72}$$

Similarly to the case of electric dipoles, the last term models magnetic dipole scattering loss, and the first term tells how much absorption loss we need in each magnetic dipole particle.

For example, assuming the Lorentz resonant model for the particle polarizability α_{ee}

$$\frac{1}{\alpha_{ee}} = \frac{\omega_{0e}^2 - \omega^2 + j\omega\Gamma_e}{A_e} + j\frac{k_0^3}{6\pi\epsilon_0} \tag{73}$$

(the last term models the radiation damping; see, e.g., Ref. [69]), we find the perfect absorption condition

$$\frac{\Gamma_e}{A_e} = \frac{\eta_0}{2}\frac{1}{S}. \tag{74}$$

From duality, we find the condition on the loss factor of resonant magnetic dipoles sitting in the same unit cells as the electric dipoles:

$$\frac{\Gamma_m}{A_m} = \frac{1}{2\eta_0}\frac{1}{S}. \tag{75}$$

The realization of a single array of resonant particles working as a perfect absorber is reported in Refs. [90,91]. In that work, a periodic planar array of right- and left-handed chiral particles is used [see Fig. 5(a)]. An equal number of right- and left-handed helices makes the effective chirality negligible, as is required for symmetric perfect absorbers, and the shape of the spirals is chosen so that the electric and magnetic polarizabilities are balanced. Figures 5(b) and 5(c) show an illustration of the response of this symmetric absorber (the design parameters are taken from Ref. [90]).

Another design for symmetric absorbers realized as an array of resonant particles is presented in Ref. [92] (the authors of Ref. [92] actually used two-layer arrays, but using the same concept it can be done also with a

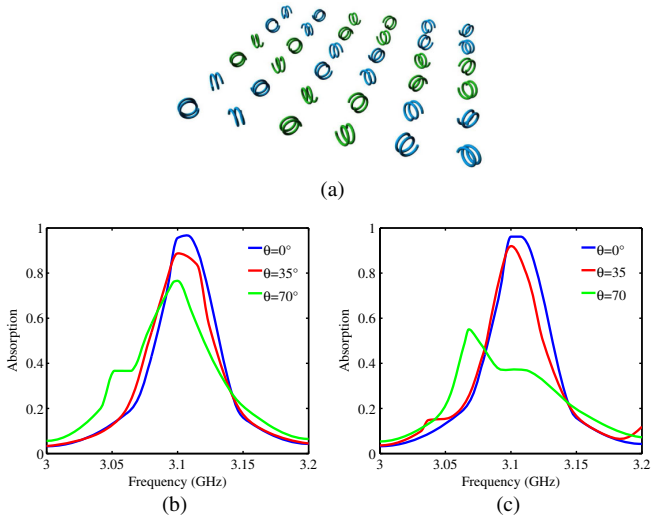

FIG. 5. (a) Topology of a symmetric absorber. Absorption at different incidence angles θ for (b) TE- and (c) TM-polarized plane-wave incidences.

single layer of resonant inclusions). Yet another proposed topology uses an array of dielectric-coated metal cylinders [93].

In the following sections, we give examples of thin asymmetric absorbers, with different response to waves incident on the two sides of the layer. As shown above, these structures realize balanced bianisotropic (omega) layers.

B. Asymmetric perfect absorbers

Asymmetric perfectly absorbing structures exhibit perfect absorption properties only for illumination from one of the two sides of the layer. The reflection coefficient of the opposite side is different from zero, and, as explained above, the layer is a bianisotropic omega structure. Although the physical operational principle of all thin asymmetric absorbers is the same, and the induced electric and magnetic surface-current densities are the same, actual topologies of the layer and the materials from which the absorber is made can vary a lot. In the following, we classify asymmetric perfect absorbers first into single arrays of electrically small dipolar inclusions in a homogeneous host (usually free space) and structures which contain a mirror or an interface (from ideally conducting surfaces to moderately lossy dielectric half-spaces). Still there is a great variety of structures which contain a ground plane, and we classify them into structures which contain an ideal or nearly ideal boundary (PEC or PMC plane) and structures which have a finite-conductivity (or moderately lossy) ground plane.

1. Arrays of resonant bianisotropic omega particles

As explained in Sec. III D, the polarizabilities (per unit cell or per unit area) of asymmetric perfectly absorbing sheets are the same as those of bianisotropic omega particles. Thus, it appears that the most natural realization of such absorbers would be in the form of periodical two-dimensional arrays of omega particles, whose collective polarizabilities are tuned to the values given by Eqs. (41)–(43). This scenario has been studied in detail in Ref. [67]. In that paper, Ω-shaped pieces of thin conducting wires are considered as possible bianisotropic omega inclusions, but it is shown that particles formed by a single Ω-shaped piece of wire are not suitable for this application. The reason for this limitation is that the different polarizabilities of such particles cannot be controlled independently, as they are related to each other (all the polarizabilities are defined by the same resonant current mode; see details in Ref. [94]). As shown in Ref. [94], this limitation can be lifted by using asymmetric particles or unit cells containing more than one conducting element. A natural choice is to use a set of two metal patches of different dimensions or shapes located close to each other, effectively forming one bianisotropic inclusion.

As an example, Fig. 6(a) shows an absorbing layer possessing omega coupling. This layer is composed by two very closely positioned arrays of different metal patches. The calculated absorptions for waves hitting different sides of the layer are shown in Fig. 6(b). The results demonstrate completely different behavior for waves coming from different sides.

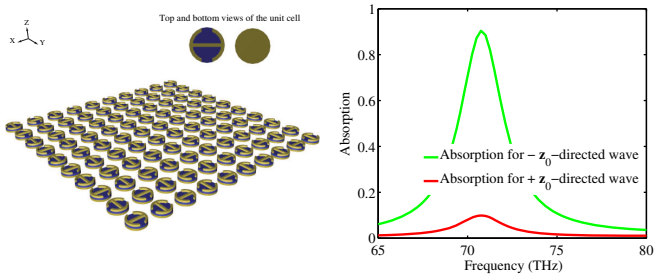

(a) (b)

FIG. 6. A typical topology of an omega layer. (a) An example of an array of resonant particles possessing omega coupling. (b) Absorption for $-z$- and $+z$-directed waves.

Topologically, the structures described in Refs. [22,46,95,96] function as omega unit cells (two arrays of asymmetric metal patches), which means that these structures can fully absorb power from one side but can have controllable reflection for the wave illuminating the opposite side (transmission must be symmetric due to reciprocity). On the other side, the structure described in Ref. [29] looks like an omega unit cell (a complex-shaped capacitive patch next to a metal strip), but in fact the dimensions of the strip array are chosen so that it behaves as a nearly perfectly conducting plane (our simulations show that within the operational frequency band the reflection coefficient of the strip array is close to 0.9, and the reflection phase is about −170°). Thus, it is one of the many realizations of high-impedance surface absorbers, described in Sec. V B 4.

There are other bianisotropic structures which were proposed to work as absorbing layers. For example, putting a symmetric dual-patch structure on top of a substrate, one can break the symmetry and introduce bianisotropic coupling in the structure [31] (see Fig. 7). However, the layers described in that paper are electrically thick. More about the use of substrate-induced bianisotropy can be found in Sec. V B 11. For most applications, illumination of only one side of the absorbing structure is relevant. Apparently for this reason, the role of bianisotropic coupling and consequently the possibilities to realize and control different responses for different sides have not been realized earlier. In many papers on asymmetric bianisotropic absorbers, e.g., Refs. [20,22,29,31,46,95,96], only absorption of waves coming from one of the two sides of the layer is considered.

Most of the known realizations of asymmetric perfect absorbers contain a ground plane or an interface between two different media, possessing high optical contrast, and we describe them next.

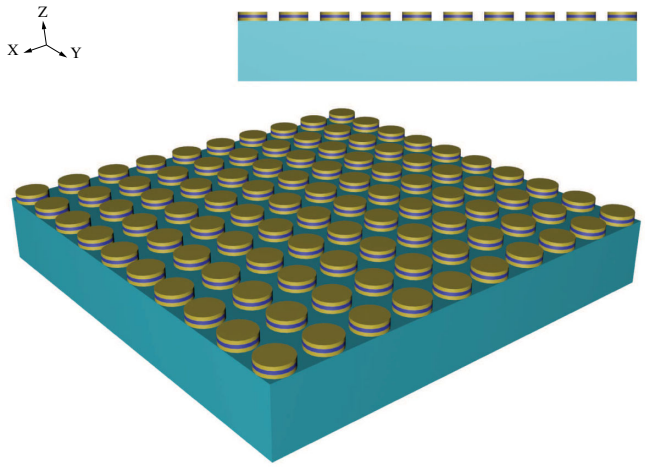

FIG. 7. Realizing omega layers positioning a symmetric patch array on top of a dielectric layer.

2. Asymmetric absorbers containing a ground plane: General considerations

Possible strategies of the realization of perfect absorbers positioned at an interface with a homogeneous medium can be conveniently understood with the use of an equivalent circuit. The input impedance and admittance of a half-space filled with an isotropic medium with the relative parameters ϵ_s and μ_s read

$$Z_s = \eta_0\sqrt{\frac{\mu_s}{\epsilon_s}} = R_s + j\omega L_s, \qquad Y_s = \frac{1}{Z_s} = G_s - jB_s \tag{76}$$

(writing in this form, we emphasize that the imaginary part of the surface impedance of metals or lossy dielectrics is inductive: $\omega L_s > 0$, $B > 0$). Asymmetric absorbers can be realized by positioning an electrically thin layer of a homogeneous or composite material on the interface surface. The electromagnetic properties of such a layer can be always modeled by a set of linear relations between the surface-averaged tangential field components on its two surfaces, in the form of a transmission matrix or impedance (admittance) matrix; see Sec. IV B 1. This modeling is possible even for composite layers (for example, arrays of complex-shaped particles) as long as the thickness of the homogeneous substrate is much larger than the period of the arrays inside the covering layer, because the effects of evanescent fields in the vicinity of the layer can be incorporated into linear relations between the fundamental propagating plane-wave fields (e.g., Ref. [69]). Furthermore, for any reciprocal layer, isotropic in the absorber plane, the impedance or admittance matrix can be presented in the form of an equivalent T circuit (or Π circuit) with effective scalar impedance and (or) admittance components. Thus, any absorber formed by a material or composite layer on an interface with another material can be modeled by the equivalent circuit shown in Fig. 8. The symmetric T circuit shown in the picture corresponds to layers without intrinsic bianisotropy (e.g., an isotropic layer on an interface). In the most general case, the two series impedances may be different.

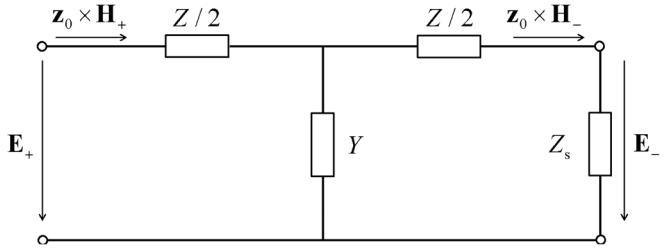

FIG. 8. Circuit model of a material layer on an arbitrary substrate. The substrate is modeled by the surface impedance Z_s, and the T circuit models a layer of an arbitrary thickness. For perfect absorption, the input impedance (ratio of the "input voltage" $\mathbf{E}_+$ and "input current" $\mathbf{z}_0 \times \mathbf{H}_+$) must be equal to the free-space impedance η_0.

For the special case when the absorbing layer is filled with a homogeneous isotropic material (permittivity $\epsilon = \epsilon_r\epsilon_0$ and permeability $\mu = \mu_r\mu_0$), the equivalent parameters read [69]

$$Z = j2\eta\tan\left(\frac{kd}{2}\right) \approx j\omega\mu d = j\eta_0\mu_r k_0 d, \tag{77}$$

$$Y = \frac{j}{\eta}\sin(kd) \approx j\omega\epsilon d = \frac{j}{\eta_0}\epsilon_r k_0 d. \tag{78}$$

Here $k_0 = \omega\sqrt{\epsilon_0\mu_0}$, $k = \sqrt{\epsilon_r\mu_r}k_0$, $\eta_0 = \sqrt{\mu_0/\epsilon_0}$, and the approximation refers to the case of electrically thin layers ($|k|d \ll 1$). The perfect-absorption conditions can be formulated in terms of matching: The parameters of the cover should be chosen so that the input impedance of the circuit would be equal to the free-space wave impedance η_0. Analyzing the equivalent circuit of Fig. 8, we see that the choice of an appropriate absorbing layer is critically dependent on the value of the surface impedance of the underlying half-space.

If the real part of the surface impedance Z_s is smaller than η_0 and the absorbing layer is electrically thin, it is obvious that we need a lossy magnetic layer, because the total input resistance must be higher than the real part of Z_s. This situation is realized in the case of highly conducting materials (such as metals at microwave frequencies) used to form the ground plane or mirror. In this case, the absorber behaves as a series resonant circuit, formed by Z_s and Z. It is difficult to find natural magnetic materials with the desired properties, and usually the way to realize this response is to use artificial magnetic layers. In the rest of the review, different ways to realize such a response are discussed. The use of dielectric layers as perfectly absorbing layers backed

by good conductors implies the use of layers of resonant thickness (the Dallenbach absorber, Sec. V B 8).

If the real part of the surface impedance is larger than η_0, adding a series resistor Z will only make it larger. It is obvious that in this case perfect absorption is possible to achieve with a thin lossy dielectric layer, acting as a shunt impedance with respect to Z_s. In this case, the absorbing structure forms a parallel resonant circuit, formed by Z_s and Y. This situation is typically realized in the case of optical frequencies and metals as materials for the ground plane, when the negative-permittivity response of metals can provide the necessary inductive response. This *internal inductance* is due to reactive magnetic-field energy stored inside the metal substrate (sometimes called *kinetic inductance*). The resonance is similar to the plasmonic resonance at an interface of metal (negative real part of the permittivity) and a dielectric or composite layer (positive permittivity), although in this case there is no surface-wave excitation. As discussed above, the resonance is necessary to make the input impedance real, and the amount of losses in the dielectric layer is chosen so that the value of the total input impedance is equal to η_0. For a detailed description of these absorbers, see Sec. V B 9.

The internal-inductance absorbers have a clear advantage of simplicity in design and realizations: In principle, the absorber can be formed just by a dielectric (semiconductor) sheet on a metal surface. It may be necessary to use some composites to realize the needed electric response, though. However, realizations of this type of absorbers are possible only when two conditions on the ground-plane surface admittance Y_s are satisfied. The first condition we have just discussed: The real part of the wave admittance of the ground-plane material should be smaller than the free-space wave admittance: $G_s < 1/\eta_0$. The second condition requires that the fields inside the ground plane decay fast (the imaginary part of $\sqrt{\epsilon_s}$ is sufficiently large). If this condition is not met, the waves in the substrate decay slowly, and, although matched, this structure is not working as a thin absorber. In practice, these restrictions limit the concept of the internal-inductance absorber to infrared and optical frequencies.

Furthermore, if the imaginary part of the permittivity ϵ_s is very large (metals at microwave frequencies, for example), the reactive part of the input impedance (the surface inductance L_s) is very small. In this case, the internal-impedance absorber scenario does not allow one to ensure practically sufficient frequency bandwidth of the absorber. Indeed, this absorber is a parallel-type resonant structure where the inductance is due to magnetic field energy stored in the ground plane (positive reactance) and the capacitance is due to the electric field energy stored in the dielectric covering layer. As is known from the theory of high-impedance surfaces [97], the relative bandwidth is proportional to $\sqrt{L_s/C}$, where C is the equivalent sheet capacitance of the cover [$\mathrm{Im}(Y) = \omega C$]. Thus, if the surface inductance is low (too large conductivity of the substrate), there is no practical possibility to create an internal-inductance absorber using a thin high-capacitance cover (a high-permittivity dielectric layer or a capacitive array). On the other hand, note that one can get both required inductive and capacitive responses by using a lossy high-permittivity material as an absorbing layer of resonant thickness. Such absorbers can be also very thin if the refractive index of the lossy layer is sufficiently high. These devices are known as Dallenbach absorbers; see Sec. V B 8.

Only in the two extreme cases of electric or magnetic sheets, when the thickness is negligible with respect to the free-space wavelength and small with respect to the wavelength inside the layer, can we model the layer as a purely electric or magnetic (capacitive or inductive) sheet. Generally, a finite-thickness material layer or a composite (metamaterial) layer stores both electric and magnetic energies, and both tangential electric and magnetic fields change across the layer, as is evident from the general equivalent circuit model of any thin absorber, shown in Fig. 8. In other words, both electric and magnetic responses in the covering layer are generally present.

In the following sections, we consider various realizations of asymmetric absorbers as homogeneous or composite layers on perfect and imperfect ground planes. We start from perfect absorbers realized as electrically thin layers of conventional lossy materials on top of a PEC or PMC ground plane.

3. Thin layer of a homogeneous magnetic material on a PEC plane

One of the classical thin microwave absorbers is a layer of a lossy magnetic material on a PEC surface. The main idea of this device comes from the fact that in the vicinity of a PEC surface the tangential magnetic field is strong (right at the PEC wall, it is twice as strong as the incident magnetic field). Thus, it appears natural to position here a slab of a lossy magnetic material to absorb the incident power. To find the required value of the permeability, we specialize the theory of Sec. V B 2 for the case when $Z_s = 0$ (PEC ground plane) and $Y = 0$ (magnetic material with $|\epsilon_r| \ll |\mu_r|$) and write the input impedance in the approximation of an electrically thin layer (thin also as compared with the wavelength inside the slab):

$$Z_{\mathrm{inp}} = j\eta_0\sqrt{\frac{\mu_r}{\epsilon_r}}\tan(k_0 d\sqrt{\mu_r\epsilon_r}) \approx j\eta_0\mu_r k_0 d \tag{79}$$

(here d is the layer thickness). Equating the input impedance (79) to the free-space impedance η_0, we find that this structure works as a perfect absorber if μ_r is imaginary and

$$\mu_r = -\frac{j}{k_0 d}. \tag{80}$$

This result appears, for example, in Ref. [6]. To check if the assumption of a small electrical thickness holds with this value of the permeability, we calculate $|k|d = k_0 d|\sqrt{\mu_r \epsilon_r}| = \sqrt{k_0 d}$. Thus, this analysis can be used under the condition $\sqrt{k_0 d} \ll 1$.

The volumetric magnetic-current density in the magnetic layer is proportional to the magnetic field inside the layer $\mathbf{H}$: $\mathbf{j}_m = j\omega(\mu - \mu_0)\mathbf{H}$. The magnetic field inside the slab varies as $\cos(kd)$, which we should approximate as a constant, because we have kept only the first-term expansion term in (79). Furthermore, since there is no reflection, this field equals the incident magnetic field: $\mathbf{H} = \mathbf{H}_{\text{inc}}$. Thus, the equivalent magnetic surface-current density reads

$$\mathbf{J}_m = \mathbf{j}_m d = j\omega\mu_0(\mu_r - 1)\mathbf{H}_{\text{inc}} d \approx \eta_0 \mathbf{H}_{\text{inc}}. \tag{81}$$

Here we have substituted the value of μ_r from Eq. (80) and neglected the real part inside the brackets. Actually, this is not an approximation: For the reference plane at the absorbing layer surface, the equivalent boundary condition reads $\mathbf{J}_m = j\omega\mu_0\mu_r d\mathbf{H}_{\text{inc}}$ (Sec. 2.5 in Ref. [69]). As expected, this value is as required for perfect absorption in thin layers [Eq. (21)].

The electric current is excited on the PEC sheet, and the exciting electric field is the sum of the incident field and the plane-wave electric field created by the magnetic-current sheet [Eq. (81)]:

$$E = E_{\text{inc}} - \frac{J_m}{2} = E_{\text{inc}} - \frac{\eta_0 H_{\text{inc}}}{2} = \frac{1}{2} E_{\text{inc}}. \tag{82}$$

This field is compensated by the field created by the electric current on the PEC surface, to fulfill the PEC boundary condition:

$$-\frac{\eta_0}{2} J_e = -\frac{1}{2} E_{\text{inc}}, \tag{83}$$

which determines the value of the electric surface-current density

$$J_e = \frac{1}{\eta_0} E_{\text{inc}}. \tag{84}$$

This result is the same value as required by Eq. (20), and we see that the two current sheets indeed form a Huygens pair.

As it was explained in Sec. III, all thin asymmetric absorbers are bianisotropic omega layers. Let us calculate the polarizabilities (per unit area) of this structure and show that it is a bianisotropic omega layer with the parameters required by the theory of Sec. III D. If we excite this absorber by a tangential uniform external electric field (while the external magnetic field is zero), the electric field will directly excite the electric current on the PEC surface, but then this current sheet will generate a plane wave, whose magnetic field will induce magnetic currents in the magnetic layer. To find the effective polarizabilities of the structure, we will utilize the same approach as in Appendix A, calculating the currents induced by uniform electric and magnetic external fields. The result of the calculations (given in Appendix B) shows that the induced electric (p_x) and magnetic (m_y) moments per unit area satisfy Eq. (24) with the coefficients

$$\bar{\bar{\hat{\alpha}}}_{ee} = \hat{\alpha}_{ee}\bar{\bar{I}}_t = \frac{1}{\eta_0}\frac{3}{2j\omega}\bar{\bar{I}}_t, \qquad \bar{\bar{\hat{\alpha}}}_{mm} = \hat{\alpha}_{mm}\bar{\bar{I}}_t = \eta_0\frac{1}{2j\omega}\bar{\bar{I}}_t, \tag{85}$$

$$\bar{\bar{\hat{\alpha}}}_{me} = \bar{\bar{\hat{\alpha}}}_{em} = j\hat{\Omega}\bar{\bar{J}}_t = -\frac{1}{2j\omega}\bar{\bar{J}}_t. \tag{86}$$

This result fully agrees with the requirements given in Sec. III D and with the result for high-impedance structures in Eqs. (46)–(48) and Appendix A. This result shows that the balance conditions between the polarizabilities hold, as should be in any thin asymmetric perfect absorber.

The simplest equivalent circuit of this absorber is of T type, as shown in Fig. 8, where the shunt admittance can be neglected (an open circuit). The value of the series impedance is equal to the sheet impedance of a thin magnetic layer (e.g., Sec. 2.5 in Ref. [69]):

$$Z = j\omega\mu_0\mu_r d. \tag{87}$$

Obviously, with the permeability value required for the perfect absorption operation (80), we have $Z = \eta_0$, and the matching condition is satisfied. If the ground plane is not ideally conducting, the total absorption condition reads

$$Z_{\text{inp}} = Z + \eta_0\sqrt{\frac{\mu_s}{\epsilon_s}} \approx j\omega\mu_0\mu_r d + \eta_0\frac{1+j}{\sqrt{2}}\sqrt{\frac{\omega\epsilon_0}{\sigma}} = \eta_0. \tag{88}$$

Here ϵ_s and μ_s are the relative parameters of the ground-plane material. The last approximate expression is for the case of a good conductor with $\epsilon_s \approx -j\sigma/(\omega\epsilon_0)$, where σ is the substrate conductivity.

As any thin absorber, this is a resonant structure (the input impedance is real in the perfect absorption regime). For a PEC ground plane, the resonance parameters are determined by the dependence of the permeability of the magnetic substrate μ_r on the frequency. In the general case of an arbitrary substrate, we have a series resonance of the surface impedance of the substrate (half-space or a more complex layered structure) and the sheet impedance of the magnetic covering layer.

Practical implementations of this design are limited by the properties of available materials, and there has been considerable effort in the synthesis of magnetic materials with high losses at microwave frequencies but with limited success, especially above 1 GHz. As an example, by using

nanostructured multilayers described in Refs. [98] or [99], it appears possible to realize absorbers of the normalized thickness $k_0 d$ of the order of $1/100$ at the frequencies up to 3–4 GHz. An extensive recent review of various magnetic materials for absorber applications can be found in Ref. [100]. Realizations of this principle at more elevated frequencies require the use of artificial magnetic materials (metamaterials and metasurfaces), which we consider next. In fact, even for applications in microwave absorbers artificial magnetics may have advantages over natural magnetics; see a review paper [101]. However, the bandwidth of absorbers [15] and material-filled small antennas [102] is determined by the static (zero frequency) value of the permeability. For example, for an absorber formed by an arbitrary isotropic material slab on a PEC plane, the fundamental limitation on the absorption bandwidth can be formulated in terms of the minimum allowed absolute value of the reflection coefficient R_0 within an interval of wavelengths from $\lambda_{\min}$ to $\lambda_{\max}$ as

$$|\ln R_0|(\lambda_{\max} - \lambda_{\min}) \leq 2\pi^2 \mu_s d, \tag{89}$$

where d is the absorber thickness and μ_s is the *static* value of the relative permeability of the absorbing material. This result clearly calls for the use of natural magnetic materials in contrast to artificial magnetics (like split-ring composites).

4. Thin layer of an artificial magnetic at a PEC plane (high-impedance surface absorbers)

As we have just noted, it is difficult or even not possible to find natural magnetic materials with the properties needed for the realization of simple absorbers described in the previous section, especially at elevated frequencies. This problem can be solved by using artificial magnetic materials or structures. Usually, these layers are thin also in terms of the number of magnetically polarizable inclusions ("metaatoms") across the layer thickness. Most commonly, only a single layer of some particles is used. Because of this, the theory of thin homogeneous magnetic layers (Sec. V B 3) cannot be applied, because the model of an equivalent bulk medium characterized by its effective permeability implies volume averaging, and, thus, it cannot be introduced for single layers of particles. The notions of the effective grid or sheet impedance, which imply only surface averaging, will be used instead.

One possible solution to realize artificial magnetic response is to use a high-impedance surface. The most common topology of high-impedance surfaces is often called the *mushroom structure* [103]. In this structure, a metal patch array is located on a thin dielectric substrate, backed by a metal ground plane; see Fig. 9. Most of these designs are for the microwave frequency range where the ground plane can be assumed to be perfectly conducting (PEC). The name "mushroom structure" comes from the original topology [103], where each patch is connected to the ground plane with a thin conducting via, forming a "mushroom." However, if this structure is excited by normally incident plane waves, there are no currents in thin vias, because the electric field is orthogonal to the wires. Thus, the vias are not needed and can be removed. The presence of vias is important for the operation at oblique incidence, where they become useful also in absorber applications; see, e.g., Refs. [19,21]. Different shapes of patches can be chosen for unit cells of mushroom arrays, but all realizations use basically the same principle.

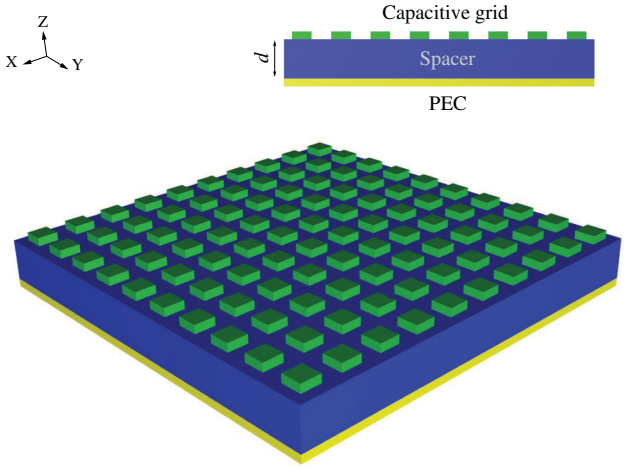

FIG. 9. A typical mushroom structure forming a high-impedance surface. No vias connectors are used in view of applications for absorbing normally incident plane waves.

In this absorber, the necessary resonant response (recall that the values of the Z-matrix parameters of perfect absorbers are purely real) is organized as a parallel-circuit resonance of the capacitive grid impedance of the array of disconnected metal patches and the inductive impedance of a short-circuited transmission line between the patch array and the PEC ground plane. At the position of the grid, the impedance matching (perfect absorption) condition can be written as

$$Y_g + \frac{1}{j\eta \tan kd} = \frac{1}{\eta_0}, \tag{90}$$

where Y_g is the grid admittance, and k and η are the wave number and wave impedance, respectively, of the substrate material. Analytical formulas to design arrays with the needed grid admittance can be found in Refs. [104,105].

The total electric currents on the PEC plane and the averaged electric currents on the patch arrays and the differential current on these two surfaces form a Huygens pair thanks to bianisotropic omega coupling in the structure. This property can be shown by deriving polarizabilities per unit area in incident electric and magnetic fields, which can be assumed to be uniform over the layer thickness. To do that, one can assume that the structure

is in the field of a standing plane wave [69] and find the induced currents satisfying the boundary conditions on the PEC plane and on the patch array. As a result, the polarizabilities per unit area in the regime of perfect absorption are found to be equal to

$$\hat{\alpha}_{ee}^{\mathrm{co}}=\frac{3}{j2\omega\eta_0},\quad \hat{\alpha}_{me}^{\mathrm{cr}}=j\hat{\Omega}=\hat{\alpha}_{em}^{\mathrm{cr}}=-\frac{1}{j2\omega},\quad \hat{\alpha}_{mm}^{\mathrm{co}}=\frac{\eta_0}{j2\omega} \tag{91}$$

(details of the derivation are given in Appendix A). It should be noted that the polarizabilities derived for the thin metamaterial-based absorbers are defined in terms of induced moments per unit area, which are related to the polarizabilities of particles in Eq. (24) as $\alpha_{ij}\to\alpha_{ij}/S$. Considering this, one can simply see that the polarizabilities satisfy the required conditions (34) and (37) for absorbing arrays of reciprocal inclusions. For a plane-wave excitation at normal incidence, we can write for the induced dipole moments per unit area

$$p=\frac{3}{j2\omega\eta_0}E_0-\frac{1}{j2\omega}H_0=\frac{1}{j\omega\eta_0}E_0,$$
$$m=\frac{1}{j2\omega}E_0+\frac{\eta_0}{j2\omega}H_0=\frac{1}{j\omega}E_0. \tag{92}$$

Obviously, this is a Huygens pair which satisfies the perfect absorption requirements (23) and (36).

Numerous particular realizations of thin absorbers of this type have been reported, e.g., Refs. [19,21,29,30,53,63,66,106]. The majority of the known realizations are for the microwave frequencies, and they use metals, most commonly, copper, as the material for the ground plane and the capacitive patch array. It is interesting to note that the circuit-analogue absorber [4] has the same topology: a patch array over a metal ground plane, but in that case the thickness of the spacer is close to $\lambda/4$, so the circuit-analogue absorber is a modified Salisbury screen. Here, the reactive response of the array is used to enhance the frequency bandwidth through double-resonance properties of the device. The same is true for an early suggestion (published in 1999) to position a patch array on a lossy, metal-backed dielectric substrate [107]. As an example of asymmetric absorbers, Fig. 10 shows the absorption spectrum for the mushroom absorber shown in Fig. 9 with the design parameters given in Ref. [21].

Alternatively to the mushroom high-impedance surface topology, an artificial magnetic layer can be realized as an array of small magnetically polarizable particles made of conductors or high-permittivity dielectrics. For instance, small resonant spirals [108] or split rings (SRRs) [109] or resonant ferroelectric inclusions [110] can be used. An example of such absorber design, where an SRR array is located on top of a ground plane covered by a thin lossy dielectric, can be found in Refs. [111,112]. Actually, in this design one can simply make the SRR array from a lossy metal, without any need for a lossy dielectric spacer.

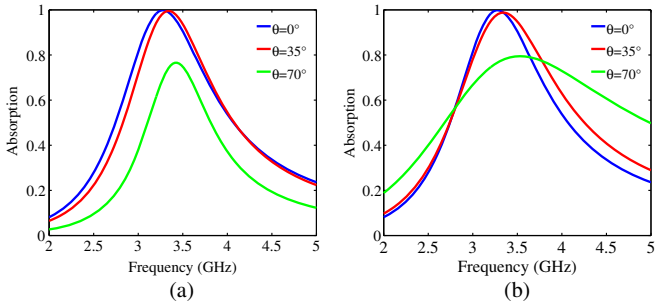

FIG. 10. An illustration of the response of an asymmetric absorber (mushroom absorber). Absorption at different incidence angles θ for (a) TE- and (b) TM-polarized plane-wave incidences.

5. External-inductance and internal-inductance absorbers

Up to now, we assumed that in high-impedance surface absorbers the ground plane behaves as a PEC surface. Let us next discuss the influence of finite conductivity (and other finite electromagnetic parameters) of the ground plane in these absorbers. This discussion is especially relevant for applications at terahertz and higher frequencies. Referring to Fig. 8, imagine a situation where the ground plane is not ideally conductive ($Z_s\neq 0$). For metals, this property means that it has a considerable inductive surface impedance in addition to some finite resistance. Fields penetrate into the ground-plane medium, and the total inductive response of the absorber structure is both due to the magnetic flux in the space between the ground plane and the patch array and due to the flux inside the ground plane itself. We can state that if the inductive response due to the magnetic fields inside the ground plane is smaller than that due to the magnetic fields in the spacer volume (inductance is mainly *external* with respect to the ground plane), the absorber can be considered as a high-impedance-surface absorber, whose operational principle is the same as of the microwave mushroom absorbers. In the opposite situation when most of the reactive magnetic field energy is stored inside the ground-plane medium (*internal inductance*), we classify these absorbers as *internal-inductance absorbers*. In the case of highly conducting ground planes at microwave frequencies, when the inductance of high-impedance surface absorbers is mainly due to the flux between the ground plane and the patch array (Sec. V B 4), the name *external-inductance absorber* is appropriate.

To understand what the physical nature of the resonance is and to which class a particular absorber belongs, one can consider the generalization of the perfect absorption condition (90) for the case of nonideal ground planes:

$$Y_g + \frac{1 + j\frac{Z_s}{\eta}\tan kd}{Z_s + j\eta\tan kd} = \frac{1}{\eta_0}. \tag{93}$$

Here we have replaced the input admittance of a short-circuited transmission line by that of a transmission line loaded by impedance Z_s, e.g., Ref. [88]. Assuming that the spacer is electrically thin (that is, $|\tan kd| < 1$), we see that if

$$|Z_s| \ll |\eta\tan kd|, \tag{94}$$

the above equation transits to Eq. (90), and we deal with a high-impedance surface (mushroom) absorber. The internal-inductance regime is realized when, in contrast, $|Z_s| \gg |\eta\tan kd|$ and, in addition, $|\frac{Z_s}{\eta}\tan kd| \ll 1$. In this case, the perfect absorption condition becomes

$$Y_g + \frac{1}{Z_s} = \frac{1}{\eta_0}, \tag{95}$$

and we deal with an internal-inductance absorber.

Most of recently reported terahertz and infrared absorbers (e.g., of Refs. [7,31,48,113,114]) are based on the high-impedance surface principle and work as external-impedance absorbers, meaning that the inductive reactance of the ground plane gives only a small addition to the main inductance due to the flux between the ground plane and the patch array. To illustrate this fact, we can consider the equivalent circuit in Fig. 8 and estimate the relevant values of the reactive impedances for some typical known designs.

As examples, we compare the structures reported in two of the papers mentioned above: Refs. [31,48]. Figures 11(a) and 11(b) compare the inductive impedance of the ground plane and the inductive impedance due to the magnetic flux in the spacer. As can be seen, the inductance provided by the metallic ground plane is considerably smaller than the one provided by the spacer, and the condition (94) is satisfied. This result clearly indicates that for the performance of these absorbers the plasmonic properties of the metal used as a ground plane are not essential, even though the metal has negative permittivity at the working frequencies and fields penetrate into the ground-plane volume.

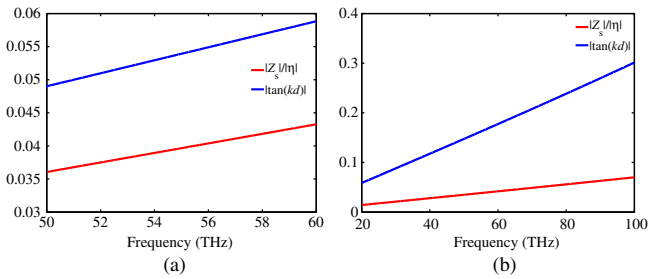

FIG. 11. Comparison between inductive impedances provided by the metallic ground plane and the spacer.

According to the above classification, these structures are high-impedance surface (mushroom) absorbers, as their operation is based on the use of the parallel-circuit resonance. The operation is defined by the same Eq. (90), with a correction due to the final conductivity of the substrate, which can be estimated by using Eq. (93). The physics behind the operation of absorbers presented in Refs. [7,113,114] is basically the same.

On the other hand, we find some examples of the structures which are closer to the internal-inductance absorber in its operational principle [64,115]. Figure 12 shows the relevant parameter values for the absorber described in Ref. [115]. One can conclude that the metallic ground plane, in the frequency region of absorption, plays the main role in providing the required inductance in comparison to the spacer. This conclusion means that the structure is working as an internal-inductance absorber. In general, the internal-inductance absorber regime is realized for substrates with $\mathrm{Re}(\sqrt{\epsilon_s}) < 1$ if the capacitive array (artificial dielectric layer) is positioned right on the metal surface, so that $|\tan(kd)|$ is very small.

6. Thin resistive sheet at an artificial PMC plane

The duality of electromagnetics suggests that it is possible to replace the PEC ground plane by a PMC ground plane and the thin layer of a lossy magnetic material by a thin layer of a lossy dielectric, to achieve the same perfect-absorption performance. To the best of our knowledge, the first absorber of this type was introduced by Schelkunoff in 1934 [116]. In that paper, he explained that to eliminate reflections from an open end of a coaxial cable (which emulates a magnetic wall) one can put a resistive sheet right at the open end of the cable. In the well-known book by Ramo and Whinnery, published in 1944, a

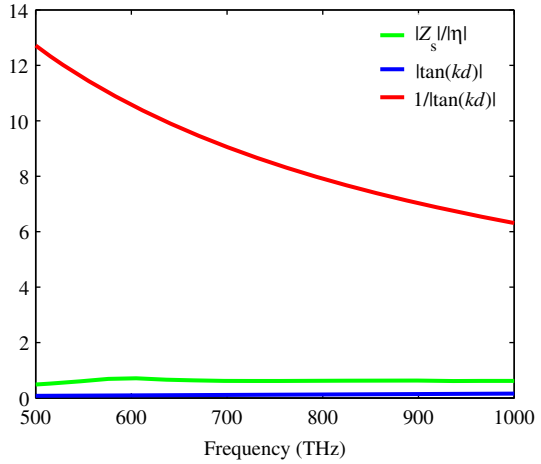

FIG. 12. Comparison between the inductive impedance provided by the metallic ground plane and the spacer for the structure presented in Ref. [115]. The internal-inductance absorber regime corresponds to $|Z_s|/|\eta| \gg |\tan(kd)|$ and, at the same time, $|Z_s|/|\eta| \ll |1/\tan(kd)|$.

topology to create this kind of absorber by positioning a resistive sheet at the $\lambda/4$ distance from a PEC ground plane is presented [75]. At this distance, the PEC ground plane is seen as a magnetic wall. In May 1943, Salisbury filed a patent application on this device, and a patent was granted in 1952 [2]. Obviously, this absorber has a considerable electrical thickness, and, since there are no naturally available magnetic conductors, this scenario of realizing thin absorbers is possible only with the use of artificial magnetic conductors.

The most common compact artificial magnetic conductor for microwave applications (more generally, HIS) is the mushroom layer: a dense array of conducting patches positioned close to a conducting ground plane [103]. We have already discussed its use as an effective lossy magnetic layer in Sec. V B 4. In the absorber type which we consider now, the mushroom layer as such is nearly lossless and used to emulate the PMC boundary. The necessary resonant response (recall that the values of the Z-matrix parameters of perfect absorbers are purely real) is organized as a parallel-circuit resonance of the capacitive grid impedance of the array of disconnected metal patches and the inductive impedance of a short-circuited transmission line between the patch array and the PEC ground plane (see Fig. 13). The PMC response takes place if the following resonance condition is satisfied:

$$Y_g + \frac{1}{j\eta_0 \tan k_0 d} = 0, \tag{96}$$

where Y_g is the grid admittance and for simplicity we assume that the volume between the patch array and the PEC plane is free space. At this frequency, the input admittance of the lossless mushroom layer is zero, and its input impedance is infinite. Analytical formulas to design arrays with the needed grid admittance can be found in Refs. [104,105].

Now, if we position a thin resistive sheet with the surface resistance equal to η_0 on the surface of this artificial magnetic wall, the absorber is matched and the incident power is fully absorbed in the resistive sheet. As we see, the only difference with the previously considered lossy mushroom structure, which emulates a lossy magnetic layer, is that here the absorption is concentrated only in the thin resistive sheet, while in the previous case it was distributed over the whole substrate volume.

To the best of our knowledge, the use of artificial magnetic conductors in thin absorbers was proposed in 2002 [27] and then experimentally verified in Ref. [11]. Various patch shapes have been proposed by many researchers, including space-filling curves [117]. Another topology to realize an artificial magnetic wall is to use an array of small spirals, split rings, or high-permittivity particles as resonant magnetic inclusions (see also the previous section). Using the same principle, one can position a resistive sheet close to such an array and achieve full absorption of electromagnetic waves [28,118]. An illustration of this topology is shown in Fig. 14.

7. Using graphene in thin absorbers

At terahertz frequencies, graphene sheets can be used as the material for patch arrays of mushroom absorbers (arrays of graphene nanodisks are described in Ref. [119], and graphene nanoribbons are used in Ref. [120]). The electromagnetic properties of graphene are usually modeled by its complex surface conductivity, which is the same as the sheet or grid admittance Y_g used in this review. Typical frequency dependence of the graphene sheet impedance, calculated by using the Kubo approximation (e.g., Ref. [121]), is shown in Fig. 15. In this example, the graphene sheet parameters are the same as in Ref. [119]: The chemical potential is 0.4 eV, the carrier lifetime is 4×10^{-13} s for both intraband and interband transitions,

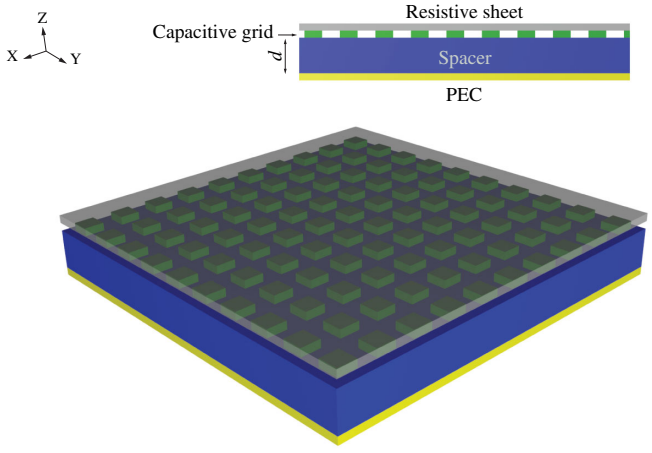

FIG. 13. A lossy sheet on top of a high-impedance surface (lossless mushroom layer).

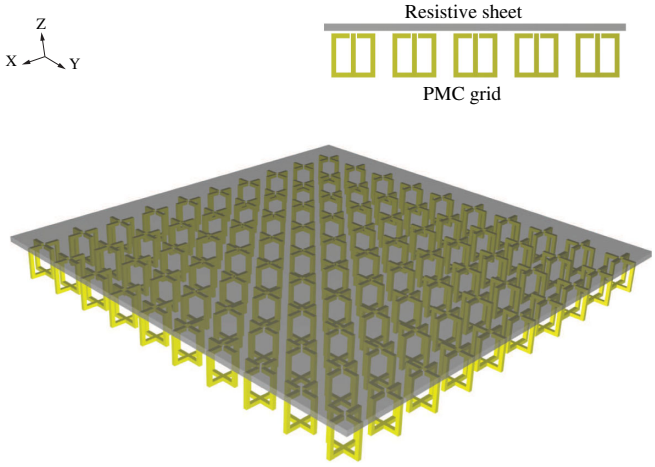

FIG. 14. A lossy dielectric layer in the vicinity of an artificial PMC surface realized as an array of resonant split rings.

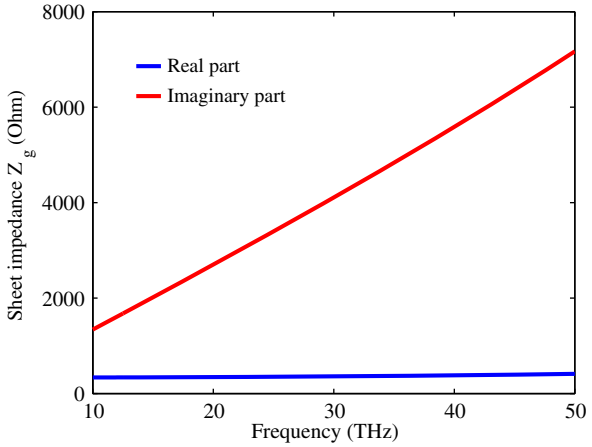

FIG. 15. Typical dependence of the graphene sheet surface impedance on the frequency in the terahertz frequency band. The MATLAB code implementing the Kubo model is used courtesy of Dr. I. Nefedov.

and the temperature is 300 K. We can observe that under these conditions the graphene sheet behaves as a moderately lossy conductor with the loss parameter (the real part of the sheet impedance) quite suitable for absorber applications. However, the significant inductive impedance of graphene needs to be compensated by some sheet capacitance, which can be provided by breaking the graphene sheets into patches [119] or strips [120] (if only one polarization is of interest). Two scenarios are, in principle, possible. The capacitance per unit area (due to gaps) can be tuned to resonate with the graphene sheet inductance, so that the total sheet impedance becomes resistive and close to the free-space wave impedance. In this scenario, the substrate thickness should be close to a quarter wavelength, and the absorber is working as a Salisbury screen. Alternatively, the total sheet reactance can be tuned to be strongly capacitive (very small gaps between graphene patches). In this scenario, the substrate thickness can be significantly smaller, and the operation is similar to the high-impedance-surface absorbers. In the example given in Ref. [119], the thickness is 1.12 μm, which is smaller than the quarter wavelength (1.6 μm) but not significantly smaller. Unfortunately, in both scenarios, the large inductive reactance of the graphene sheet reduces the absorber bandwidth (because some reactive energy is stored in this inductor; see Ref. [97]), and, thus, the use of metals in terahertz absorbers appears to be preferable to graphene.

Graphene layers can be also used to achieve tunability of absorbers. For example, in Ref. [122], a double layer of graphene strips was embedded into a lossy dielectric substrate of a high-impedance-surface terahertz-frequency absorber (a capacitive array of golden patches on a metal-backed lossy dielectric substrate, Sec. V B 4). Modulating the graphene surface impedance by using voltage bias, the resonant frequency of the device can be changed.

8. Dallenbach absorbers

As we saw from the general considerations of absorbing layers on PEC ground planes (Sec. V B 2), to realize a thin absorber we need to use magnetic layers (natural or artificial). An absorbing layer made of a purely dielectric material must have a considerable (in fact, resonant) electrical thickness. However, if the permittivity of the material is high, the layer thickness can be still small as compared with the free-space wavelength. This absorber is one of the classical designs (see Fig. 16), and it is called the Dallenbach absorber [1,5,123]. The requirements on the material parameters and thickness can be found by equating the input impedance of the layer (thickness d and relative permittivity ϵ_r) on a PEC ground plane to the free-space wave impedance:

$$Z_D = j\eta_0 \frac{1}{\sqrt{\epsilon_r}} \tan(k_0 d\sqrt{\epsilon_r}) = \eta_0. \tag{97}$$

The input impedance takes real values at the thickness resonances (the lowest one, at the quarter-wave thickness). The loss parameter should be chosen so as to ensure matching with free space. In terms of the refractive index of the dielectric material $n = n' - jn''$, the conditions read

$$n' \approx \frac{\pi}{2k_0 d}, \qquad n'' \approx \frac{2}{\pi} \tag{98}$$

(e.g., Sec. 12.3 in Ref. [5]).

A detailed analysis of the physical mechanism behind the operation of the Dallenbach absorber is presented in Appendix C, where it is shown that close to the resonant frequency the expressions for the input impedance of a Dallenbach absorber have the same form as those for a lossy high-impedance (mushroom) layer. Furthermore, in the same Appendix, it is shown that the induced electric and magnetic moments in the Dallenbach type absorbers read

$$\begin{aligned} p_x &= \frac{2jE_0}{\xi\omega\eta_0} \frac{[F(2 - jk_0 d) - 1 + \frac{jk_0 d}{2}]}{(1 - jk_0 d)}, \\ m_y &= \frac{2jE_0}{\xi\omega} \frac{[F(2 - jk_0 d) - 1 + \frac{jk_0 d}{2}]}{(1 - jk_0 d)} \end{aligned} \tag{99}$$

(the notations are defined in the Appendix). These equations show that the condition of the Huygens layer $m_y = \eta_0 p_x$ is fulfilled. The induced electric and magnetic moments are balanced, as is required by the general theory of thin absorbers presented above. In practice, the main challenge is to find (or realize as a metamaterial) a dielectric with the refraction index approximately satisfying Eq. (98) at the design frequency and in as wide a frequency range as possible.

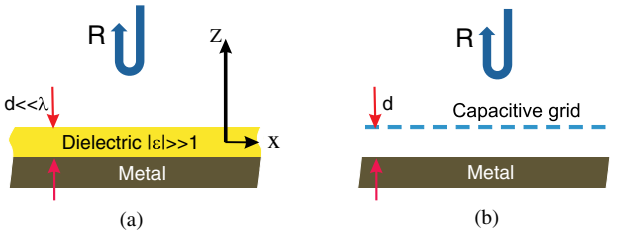

FIG. 16. (a) Geometry of a dielectric Dallenbach absorber. (b) An equivalent model as a lossy capacitive grid over the same ground plane.

9. Thin layers on imperfectly conducting surfaces: Internal-inductance perfect absorber

Let us next apply the general theory of absorbing layers on imperfect ground planes (Sec. V B 2) to the case when the ground-plane material is a plasmonic metal (thin absorbers for infrared and visible frequencies). The equivalent circuits of these structures can be considered as dual with respect to the equivalent circuit of thin magnetic-layer absorbers on good conductors: Instead of a series resonance, here we will have a parallel-circuit resonance. Indeed, the surface impedance of a conducting half-space is inductive [the imaginary part of the surface admittance Y_s is negative (76)]. Thus, it appears to be possible to cancel its reactance by capacitive reactance of a thin dielectric layer positioned on the conductor surface. The equivalent sheet admittance of a thin dielectric layer reads (Sec. 2.5 in Ref. [69])

$$Y_g = \frac{j}{\eta_0}(\epsilon_r - 1)k_0 d. \tag{100}$$

The appropriate equivalent circuit of this absorber is like shown in Fig. 8, where the series impedance Z can be neglected (approximated by zero). The total admittance of the parallel connection is

$$Y_{\text{inp}} = Y_s + Y_g, \tag{101}$$

and the perfect-absorption condition reads

$$\sqrt{\epsilon_s} + j(\epsilon_r - 1)k_0 d = 1 \tag{102}$$

[the branch of the square root is defined by $\text{Re}(\sqrt{\cdot}) \geq 0$].

Unfortunately, from here we see that for microwave absorbers this scenario requires active covering layers. For good conductors and microwave frequencies $\epsilon_s \approx -j\sigma/(\omega\epsilon_0)$, where σ is the metal conductivity. Because in this case $\sigma \gg \omega\epsilon_0$, the real part of $\sqrt{\epsilon_s} \gg 1$, and, thus, it is not possible to reduce it to the free-space level by adding some positive equivalent resistance of the covering layer.

However, this scenario is realizable in the visible range, where metals no longer behave as nearly perfect conductors. Assuming the Drude model of plasmonic metals

$$\epsilon_s = 1 - \frac{\omega_p^2}{\omega(\omega - j\Gamma)}, \tag{103}$$

the perfect-absorption condition Eq. (102) can be expressed as

$$\sqrt{\frac{\omega^2 - \omega_p^2 - j\omega\Gamma}{\omega^2 - j\omega\Gamma}} + j(\epsilon_r - 1)k_0 d = 1. \tag{104}$$

It appears that if $|\omega^2 - \omega_p^2| < \omega^2$, the real part of $\sqrt{\epsilon_s}$ is smaller than unity, and it is possible to realize a perfect absorber as a thin dielectric (semiconductor) cover. A similar design is presented in Ref. [124] without realizing the possibility of perfect absorption using this design, and an experimental demonstration of nearly perfect absorption according to this scenario was recently published in Ref. [125].

Using the experimental data on the permittivity of metals found in Ref. [126], one can see that for silver ground planes $\text{Re}(\sqrt{\epsilon_s}) < 1$ holds in the frequency range from 113 to 945 THz and for gold from 130 to 612 THz. As an example, Fig. 17 illustrates theoretical performance of perfect internal-inductance absorbers realized by positioning dielectric layers with the thickness equal to $\lambda_0/20$ on a gold substrate. The design was made for a number of frequencies within the allowed range by selecting the dielectric layer permittivity in accord with Eq. (102). To model gold properties, the data from Ref. [126] are used.

Notice that the bandwidth of these absorbers becomes smaller at lower frequencies, as expected (surface inductance decreases, which leads to a smaller bandwidth of the

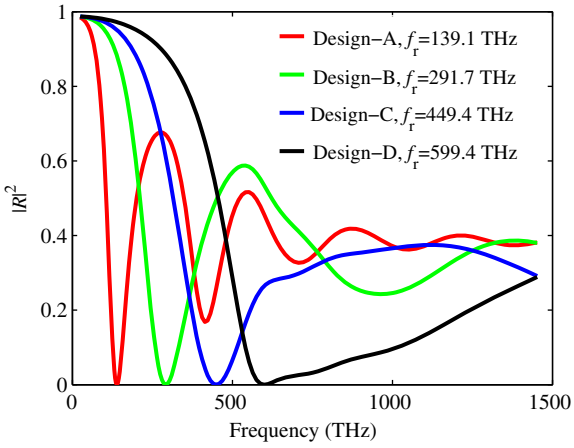

FIG. 17. Reflection coefficients from perfect internal-inductance absorbers formed by thin dielectric layers on a gold substrate. Different curves correspond to different required permittivities of the dielectric cover. Design A, $\epsilon_r = 17.1368 - j4.8309$; design B, $\epsilon_r = 12.2021 - j4.2609$; design C, $\epsilon_r = 8.5919 - j3.8204$; design D, $\epsilon_r = 5.6498 - j1.8296$. The dielectric layer thickness equals $\lambda_0/20$ at the resonant frequency of the corresponding design.

parallel-circuit resonance). Note also that, while the electrical thickness of the dielectric cover is small with respect to the free-space wavelength, it is not necessarily small compared to the wavelength inside the dielectric. In fact, for the designs at the lower end of the allowed frequency range, the optical thickness of the layer is close to the quarter-wave resonance (for design A the thickness is approximately 0.21λ), which means that the operation mechanism in this case is closer to that of the Dallenbach absorber than to the internal-inductance one. Furthermore, internal-inductance absorbers can be classified as thin absorbers only if the skin depth of the metal ground plane is small enough, so that the fields in the substrate decay at a subwavelength depth. Finally, since it is difficult or even not possible to find dielectric materials with the required permittivities (the above illustrative designs assume dispersion-free dielectric properties), some artificial dielectrics, usually in the form of arrays of electrically polarizable inclusions, need to be designed. Note that large values of the permittivity in our examples correspond to semiconductors, but real semiconductors are dispersive media and their dispersion may be not favorable for satisfying Eq. (102) with so small a thickness as $d = \lambda_0/20$.

10. Plasmonic absorbers

Perfect absorption at infrared and possibly optical range can be realized also by using arrays of resonant plasmonic nanoparticles, separated by a thin dielectric substrate from a metal ground plane. As discussed above, if the real part of the refractive index of the ground-plane metal is larger than unity (which is the case of most metals up to the infrared range), the structure which is put on top of a metal surface must possess some effective magnetic response (referring to Fig. 8, the series resistance Z is significant for absorber operation). Because the surface impedance of the ground plane Z_s is inductive, this structure should also provide some electric-polarization (capacitive) response in order to compensate the inductive reactance of the interface with the ground plane. Two distinct regimes are possible: The spacer and the plasmonic-particle array are far from the resonance, so that the reactive energy stored inside and in the near vicinity of plasmonic nanoparticles is predominantly electric. In this regime (realized in Refs. [7,37,113]), most of the inductance is due to the magnetic flux in the dielectric spacer, and the absorber's operation principle is similar to that of a high-impedance (mushroom-type) absorber. In the other possible regime, the array of plasmonic particles is close to the resonance, in which case the reactive magnetic energy is mainly in the particle array. In these structures, most of the power is lost in the resonating nanoparticles, and the operational principle is more similar to the Dallenbach absorber. This similarity means that the structure on top of a reflecting ground plane provides the phase shift equivalent to a quarter-wave gap between the interface and the ground plane. Depending on the operational frequency and used materials, intermediate mixed regimes are possible. As discussed in the previous subsection, some metals in the visible range have the real part of the surface admittance smaller than the inverse of free-space impedance. In this case, the needed dielectric-sheet response of the absorbing cover given by Eq. (102) corresponds to a semitransparent material with realistic complex permittivity. If a natural material with the needed properties cannot be found, this response can be achieved for a dielectric-semiconductor composite or even emulated by a planar array of metal particles. The topology of such absorbers (realized in Refs. [114,115,127]) is the same as for the case of resonant plasmonic arrays.

11. Metamaterial absorber based on the effect of substrate-induced bianisotropy

We see that the presence of magnetic polarization in thin layers is a necessary condition for perfect absorption. In the examples above, we see a number of techniques used to ensure the required magnetic response: the use of natural magnetic materials, artificial magnetic conductors in the form of mushroom layers, resonant split rings, small spirals, and dielectric nanospheres in the magnetic Mie resonance. Here we discuss another possibility, offered by the bianisotropic response of arrays of small particles on a transparent substrate (see Fig. 18). Clearly, bianisotropy results in effective magnetic surface polarization generated by the incident electric fields. The physical mechanism underlying this effect is called substrate-induced bianisotropy (SIB) [128].

Consider a regular planar array of plasmonic nanoparticles located at a small distance d over a transparent substrate with the relative permittivity ϵ_r [128]. Let the bottom parts of these particles be curved (e.g., as spheres or spheroids). In the plasmon resonance band, the electric field is concentrated within a hot spot which is partially located inside the nanoparticle but partially in the substrate. Local polarization currents in these two parts of the hot spot have opposite directions, because the real part of the complex permittivity of plasmonic metals is negative and that of the substrate is positive. If the absolute values of these permittivities are comparable to each other, the polarization of the hot spot (which is locally dominating over the polarization of the remainder of a unit cell) can be adequately presented as a pair of electric dipoles with comparable amplitudes and opposite directions. The effective distance between these two dipoles is close to the hot spot size. This phenomenon is nothing but generation of a local magnetic moment linked to the hot spot. In other words, the array acquires bianisotropic omega coupling. In the presence of SIB the array of plasmonic nanoparticles is fully equivalent to an array of omega particles [129]. In Ref. [130], it was shown that the SIB effect may allow satisfaction of the zero reflection condition (36), together with the zero transmission condition (37). Since the

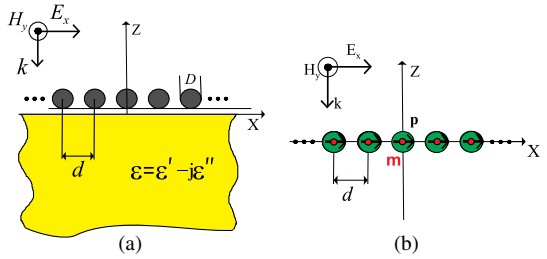

FIG. 18. (a) Horizontally isotropic grid of silver nanospheres located at a very small distance d from a semiconductor substrate. (b) An equivalent array of scatterers with both electric and magnetic responses which are balanced at a certain frequency. The action of the substrate at this frequency is modeled by the magnetic polarizability.

magnetic polarizability of nanoparticles is negligible, for metamaterial absorbers operating due to the SIB effect one should assume $\hat{\alpha}^{co}_{mm} = 0$ in both Eqs. (36) and (37). These conditions can be satisfied simultaneously within the plasmon resonance band of the original nanosphere array if $\epsilon_r \gg \epsilon_u$ (where $\epsilon_u \geq 1$ is the relative permittivity of the upper half-space) and $0 < d \ll D$, and the array period p satisfies $p \ll \lambda$. Practically, the structure from Ref. [130] may be realized of silver or gold nanospheres floating in a liquid over the surface of a semiconductor.

VI. SUMMARY AND OUTLOOK

Based on the analysis of the possible physical mechanisms of perfect absorption in optically thin structures, we can classify all known perfect and nearly perfect thin absorbers into the following categories:

(1) Symmetric absorbers (electric and magnetic resistive sheets at the same plane)
  (a) A lossy layer of a material with $\epsilon_r = \mu_r$
  (b) Arrays of resonant electric and magnetic dipoles (spirals, dipoles and split rings, etc.)
(2) Asymmetric absorbers (bianisotropic omega layers)
  (a) Arrays of resonant omega particles
  (b) Lossy layers on ideal boundaries
    (i) Thin lossy magnetic layer (natural or artificial magnetic, commonly in the form of a mushroom structure) on a PEC ground plane
    (ii) Resistive sheet on an artificial magnetic conductor surface (e.g., lossless high-impedance structure)
    (iii) Resonant lossy dielectric layer on a PEC ground plane (the Dallenbach absorber)
  (c) Layers on imperfect boundaries
    (i) Thin lossy dielectric layer (natural or artificial dielectric) on a conductor surface (internal-impedance absorber)
    (ii) Lossy artificial magnetic conductor (e.g., mushroom structure with a lossy dielectric substrate)

Symmetric absorbers as lossy layers of materials with equal relative permittivity and permeability (Sec. V A 1), being conceptually very simple, are problematic due to very strict requirements on the material parameters. Although considerable progress has been achieved in synthesizing lossy magnetic materials (e.g., Ref. [100]), there are only limited options and mainly at microwave frequencies. Symmetric perfect absorbers in the form of arrays of resonant particles (Sec. V A 2) appeared only recently, and the only known experimental realization [91] is in the microwave frequency range. Realizations in the optical range need electrically small resonant particles with balanced resonant electric and magnetic moments. Similar requirements hold for particles (metaatoms) needed for realizations of double-negative metamaterials, and considerable experience of many groups working in that field can be useful in designing perfect absorbers of this class. Various topologies, such as core-shell nanoparticles or double patches of various shapes, have been proposed and studied in the regime of as low a dissipation loss as possible. To approach the problem of perfect absorption realization, dissipation losses should be significant and controllable in the design and manufacturing.

Interestingly, while there is a huge literature on high-impedance surface (mushroom-type, Sec. V B 4) absorbers in the form of various periodical structures on top of a conducting surface, some of the simplest possible realizations of perfect absorbers have not yet been sufficiently studied. In particular, we mean internal-impedance perfect absorbers: thin lossy dielectric or artificial-dielectric sheets on a plasmonic metal or another conductor with low conductivity and high surface inductance, and we expect interesting new developments in these areas.

In the design of thin broadband absorbers, the fundamental limitation Eq. (89) suggests the use of natural magnetic materials with high static values of permeability. However, such materials are not practical in terahertz and optical devices. In this respect, a largely unexplored possibility is making use of active and parametrically pumped layers, as a route to overcome the fundamental limitations on the performance of passive absorbers. Reference [131] discusses the general conditions of zero backscattering from small particles, showing interesting new possibilities offered by active inclusions. The active route is especially promising in view of a possibility to overcome the frequency bandwidth limitations for all passive absorbers. Some initial work on active non-Foster absorbers can be found in Refs. [18,132–134]. Alternatively, frequency-bandwidth limitations can be overcome by making the absorber's parameters tunable by some external fields (most commonly, electric bias or light illumination). This route is being actively explored especially for microwave absorbers; see the review paper Ref. [135].

In this review, we discuss only perfect absorption of normally incident waves. The angular stability of thin

absorbers presents another challenge which needs further studies. Here, we expect that the key to success will be learning how to engineer spatial dispersion in metasurfaces. The use of active elements can offer an alternative route. It is important that for perfect absorption at a fixed but oblique incidence angle there are more open possibilities than for the normal-incidence case. An interesting example can be found in Ref. [136], where in the extremely thin absorbing layer the equivalent surface electric and magnetic currents are not balanced, and the necessary asymmetry in radiation of the induced currents is ensured by an infinitesimally thin layer of induced electric polarization which is directed normally to the absorbing surface.

Another possibility to improve performance of thin absorbers is to make use of amorphous arrangements of absorbing elements. Nearly all known approaches exploit periodical arrays of various topologies (possible deviations from periodicity are commonly considered as unavoidable imperfections in manufacturing). However, it appears that properly engineered randomness of metasurfaces may offer possibilities to control and potentially improve absorption efficiency. Recently, some initial studies of absorption in resonant amorphous metasurfaces were published, e.g., Refs. [64,127,137,138], but more studies and a better understanding of such structures is needed to enable optimal use of randomness in absorber design. Research in this area is motivated also by technological advantages, since amorphous metasurfaces can be manufactured by using effective and cheap bottom-up methods [138]. On the other hand, we should note that, while the use of random structures may help in controlling the absorption level and increasing absorption bandwidth, this way it is not possible to realize perfectly nonreflecting absorbers. Amorphous absorbers inevitably create some diffuse scattering in all directions, which cannot be eliminated by any matching structures.

VII. CONCLUSIONS

The general consideration of physical mechanisms of perfect absorption brings us to a number of important conclusions. First, all optically thin absorbers are based on the same principle of an absorbing Huygens sheet formed by induced electric and magnetic surface currents. Second, absorbers which equally absorb waves coming from the two sides of the sheet are simple combinations of an electric resistive sheet and a magnetic resistive sheet (no bianisotropic coupling in the layer). Third, reciprocal absorbers which absorb waves only from one side of the sheet (e.g., absorbers on a perfectly conducting ground plane) are lossy and resonant bianisotropic omega layers. As is clear from the above wide overview of different topologies which can be used to create a thin absorber, all of these absorbers are basically following the same physical concept.

Knowing the required response of thin absorbing sheets allows the use of metamaterial and metasurface synthesis methods to design particular devices. In order to realize a thin perfect absorber, one must ensure that the structure responds both electrically and magnetically and the strength of these responses is balanced at the working frequency to have zero reflection. At the same time, these induced currents should be strong enough to cancel the incident wave in the forward direction and ensure zero transmission. Having a magnetic response for an absorber structure is a necessary condition for perfect absorption. All passive thin perfect absorbers are resonant structures, which fundamentally limits their operational frequency band.

The majority of the known designs of perfect absorbers are based on only numerical simulations and optimizations. We hope that the general framework theory and the wide overview of known approaches to realizing perfect absorption in thin layers which we present here will be useful for future research in this field and for practical device development.

ACKNOWLEDGMENTS

This work was supported in part by the Nokia Foundation.

APPENDIX A: POLARIZABILITIES OF HIGH-IMPEDANCE SURFACE PERFECT ABSORBERS

Here we provide detailed derivations of polarizabilities for a typical thin absorber made of a capacitive grid mounted close to a metal sheet. Deriving induced electric and magnetic moments, it is shown that these layers act as the Huygens' layer. To find the polarizabilities, we need to excite the absorber layer by the electric field and magnetic field which are approximately constant inside the layer [69]. We choose the exciting field in the form of a standing wave as

$$\mathbf{E} = [E_0 e^{-jk_0 z} - E_0 e^{+jk_0 z}]\mathbf{x}_0 = -j2E_0 \sin(k_0 z)\mathbf{x}_0,$$
$$\mathbf{H} = [H_0 e^{-jk_0 z} + H_0 e^{+jk_0 z}]\mathbf{y}_0 = 2H_0 \cos(k_0 z)\mathbf{y}_0. \quad \text{(A1)}$$

To study the excitation by external electric fields, we position the layer so that the maximum of the electric field distribution of the standing wave is located at the middle point between the grid and the ground plane (Fig. 19), where $\sin(k_0 z) = -1$, for example, assuming $k_0 z = -\pi/2$ (the normalized distance between the grid and the ground plane is $k_0 d \ll 1$). Next, we write the relations between the averaged surface-current density on the ground plane J_{met} and on the array of patches J_g and the total surface-averaged electric fields at the respective two planes:

$$j2E_0 \cos\left(\frac{k_0 d}{2}\right) - \frac{\eta_0}{2} J_g - \frac{\eta_0}{2} J_{\text{met}} e^{-jk_0 d} = Z_g J_g,$$
$$j2E_0 \cos\left(\frac{k_0 d}{2}\right) - \frac{\eta_0}{2} J_g e^{-jk_0 d} - \frac{\eta_0}{2} J_{\text{met}} = 0. \quad \text{(A2)}$$

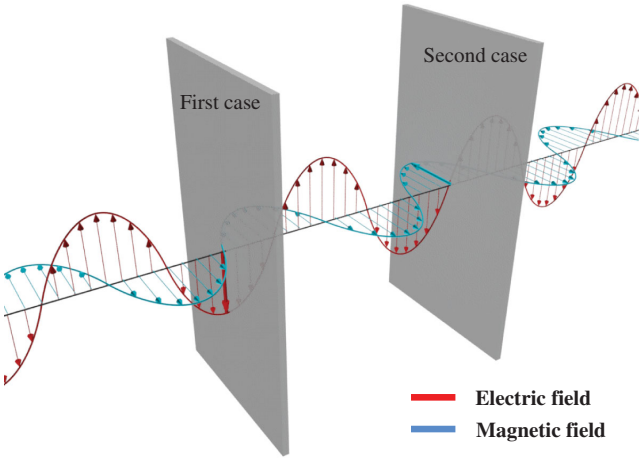

FIG. 19. Geometry of the problem. The gray plates show two test positions of the absorbing structure in the field of a standing wave.

Here Z_g is the grid impedance of the patch array. The value of the grid impedance we choose so that the absorber matches to the free space. Using the perfect-absorption condition (90), we find the required grid impedance

$$Z_g = j\eta_0\left(\frac{\sin k_0 d}{j\sin k_0 d - \cos k_0 d}\right). \tag{A3}$$

Using Eq. (A2), the currents on the patch grid and on the metal surface can be found:

$$J_{\text{met}} = j\frac{4}{\eta_0}E_0\cos\frac{k_0 d}{2} - J_g e^{-jk_0 d},$$
$$J_g = \frac{-2E_0 e^{-j(k_0 d/2)}\sin k_0 d}{j\eta_0 e^{-jk_0 d}\sin k_0 d + Z_g}. \tag{A4}$$

Substituting Z_g from (A3), we can write the surface-current density at the patch array as

$$J_g = \frac{-2E_0 e^{-j(k_0 d/2)}}{j\eta_0(-j2\sin k_0 d)} = \frac{-E_0 e^{-j(k_0 d/2)}}{\eta_0 \sin k_0 d}. \tag{A5}$$

The induced electric moment per unit area of the structure, by definition [139], reads

$$p_x = \frac{1}{j\omega}(J_{\text{met}} + J_g). \tag{A6}$$

Substituting Eqs. (A4)–(A6), we find

$$p_x = \frac{1}{j\omega}\left[j\frac{4}{\eta_0}E_0 - \frac{E_0 e^{-j(k_0 d/2)}(1 - e^{-jk_0 d})}{\eta_0 \sin k_0 d}\right]. \tag{A7}$$

Assuming that the layer is optically thin ($k_0 d \ll 1$), the above result simplifies to

$$p_x = \frac{3}{\omega\eta_0}E_0. \tag{A8}$$

Dividing the induced electric moment by the amplitude of the external electric field $j2E_0$ in Eq. (A1), we find the effective electric polarizability per unit area:

$$\hat{\alpha}_{ee}^{\text{co}} = \frac{p_x}{j2E_0} = \frac{3}{j2\omega\eta_0}. \tag{A9}$$

By definition [139], the induced magnetic moment per unit area can also be written as

$$m_y = -\frac{d\mu_0}{2}(J_{\text{met}} - J_g). \tag{A10}$$

Using Eqs. (A4), (A5), and (A10), we find the induced magnetic moment as

$$m_y = -\frac{d\mu_0}{2}\left[j\frac{4}{\eta_0}E_0 + \frac{E_0 e^{j(k_0 d/2)}(1 + e^{-jk_0 d})}{\eta_0 \sin k_0 d}\right]. \tag{A11}$$

The assumption of an optically thin layer simplifies this relation to

$$m_y = -\frac{E_0}{\omega}. \tag{A12}$$

Next, dividing the magnetic moment by the amplitude of the exciting electric field in Eq. (A1), we can calculate the magnetoelectric polarizability (omega coupling coefficient):

$$\hat{\alpha}_{me}^{\text{cr}} = \frac{m_y}{j2E_0} = \frac{-1}{j2\omega}. \tag{A13}$$

In the second step, we derive the effective magnetic and electromagnetic polarizabilities by considering excitation of the same layer by external magnetic fields. To do that, we position the layer inside the standing wave Eq. (A1) so that the maximum of the magnetic field is in between the array of patches and the ground plane, as shown in Fig. 19 (e.g., at $k_0 z = 0$). Similarly to the above, writing the relations between the induced averaged surface currents and the electric fields in the plane of the patches and the ground plane, we get

$$-j2E_0\sin\left(\frac{k_0 d}{2}\right) - \frac{\eta_0}{2}J_g - \frac{\eta_0}{2}J_{\text{met}}e^{-jk_0 d} = Z_g J_g,$$
$$j2E_0\sin\left(\frac{k_0 d}{2}\right) - \frac{\eta_0}{2}J_g e^{-jk_0 d} - \frac{\eta_0}{2}J_{\text{met}} = 0. \tag{A14}$$

From these equations we find the induced current densities on the metal surface and on the grid array:

$$J_{\rm met} = j\frac{4}{\eta_0}E_0 \sin\frac{k_0 d}{2} - J_g e^{-jk_0 d},$$
$$J_g = \frac{-j2E_0 e^{-j(k_0 d/2)} \sin k_0 d}{j\eta_0 e^{-jk_0 d} \sin k_0 d + Z_g}. \quad \text{(A15)}$$

By using Eqs. (A3) and (A15), the patch-array current can be written as

$$J_g = \frac{-j2E_0 e^{-j(k_0 d/2)} \sin k_0 d}{j\eta_0 e^{-jk_0 d} \sin k_0 d + j\eta_0 (\frac{\sin k_0 d}{j \sin k_0 d - \cos k_0 d})}, \quad \text{(A16)}$$

which for thin layers simplify to the following expression:

$$J_g = \frac{-jE_0 e^{-j(k_0 d/2)}}{\eta_0 \sin k_0 d}. \quad \text{(A17)}$$

The electric moment per unit area is calculated by using Eq. (A6):

$$p_x = \frac{1}{j\omega}\left[j\frac{4}{\eta_0}E_0 \sin\frac{k_0 d}{2} - \frac{jE_0 e^{-j(k_0 d/2)}(1 - e^{-jk_0 d})}{\eta_0 \sin k_0 d}\right]. \quad \text{(A18)}$$

Assuming an optically small thickness for the structure, we get

$$p_x = \frac{H_0}{j\omega}. \quad \text{(A19)}$$

The coupling coefficient can be found by dividing the induced electric moment by the amplitude of the external magnetic field in Eq. (A1):

$$\hat{\alpha}^{\rm cr}_{em} = \frac{p_x}{-2H_0} = \frac{-1}{j2\omega}. \quad \text{(A20)}$$

By using Eqs. (A4), (A5), and (A10), the magnetic moment can be written as

$$m_y = -\frac{d\mu_0}{2}\left[j\frac{4}{\eta_0}E_0 \sin\frac{k_0 d}{2} + \frac{jE_0 e^{-j(k_0 d/2)}(1 + e^{-jk_0 d})}{\eta_0 \sin k_0 d}\right], \quad \text{(A21)}$$

and within the same assumption of optically small thickness,

$$m_y = \frac{\eta_0 H_0}{j\omega}. \quad \text{(A22)}$$

The magnetic polarizability can be determined by dividing the induced magnetic moment by the external magnetic field in Eq. (A1):

$$\hat{\alpha}^{\rm co}_{mm} = \frac{m_y}{2H_0} = \frac{\eta_0}{j2\omega}. \quad \text{(A23)}$$

Finally, the collective polarizabilities per unit area of thin high-impedance surface absorbers can be written as

$$\hat{\alpha}^{\rm co}_{ee} = \frac{3}{j2\omega\eta_0}, \quad \hat{\alpha}^{\rm cr}_{me} = j\hat{\Omega} = \hat{\alpha}^{\rm cr}_{em} = -\frac{1}{j2\omega}, \quad \hat{\alpha}^{\rm co}_{mm} = \frac{\eta_0}{j2\omega}. \quad \text{(A24)}$$

These expressions show that there is bianisotropic omega coupling in thin metasurface-based absorbers. It should be noted that the above polarizabilities are defined in terms of induced moments per unit area, which are related to the polarizabilities of particles in Eq. (24) as $\alpha_{ij} \to \alpha_{ij}/S$. Considering this, one can simply see that these polarizabilities satisfy the required perfect-absorption conditions (34) and (37) written for absorbing using an array of individual reciprocal inclusions.

This equivalence can be expressed also in terms of induced electric and magnetic surface currents. Assuming a plane wave traveling in the $\mathbf{z}_0$ direction, the induced electric and magnetic moments in thin-layer absorbers can be written as

$$p_x = \hat{\alpha}^{\rm co}_{ee}E_x - \hat{\alpha}^{\rm cr}_{me}H_y,$$
$$m_y = \hat{\alpha}^{\rm cr}_{me}E_x + \hat{\alpha}^{\rm co}_{mm}H_y, \quad \text{(A25)}$$

where $E_x = E_0$ and $H_y = E_0/\eta_0$. Finally, substituting the polarizabilities, we find

$$p_x = \frac{3}{j2\omega\eta_0}E_0 - \frac{1}{j2\omega}H_0 = \frac{1}{j\omega\eta_0}E_0,$$
$$m_y = \frac{1}{j2\omega}E_0 + \frac{\eta_0}{j2\omega}H_0 = \frac{1}{j\omega}E_0. \quad \text{(A26)}$$

We can conclude that these form a Huygens's pair and satisfy the required perfect-absorption conditions (23) and (36).

APPENDIX B: POLARIZABILITIES OF A THIN MAGNETIC LAYER AT A PEC PLANE

Here we give details of derivations of polarizabilities (per unit area) of an asymmetric perfect absorber formed by a lossy magnetic-material layer at an ideally conducting mirror (Sec. V B 3). The geometry of the structure is illustrated by Fig. 20, and the configuration of the probe fields is the same as shown in Fig. 19.

Let us suppose that we excite this structure only by a uniform electric field $\mathbf{E} = E_0\mathbf{x}$. In this scenario, the induced electric (p_x) and magnetic (m_y) moments per unit area can be written as

$$p_x = \hat{\alpha}_{ee}E_0, \qquad m_y = \hat{\alpha}_{me}E_0. \quad \text{(B1)}$$

The boundary condition on the PEC surface reads

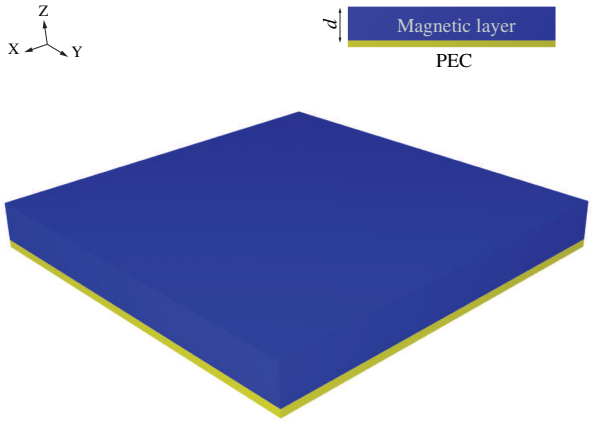

FIG. 20. Magnetic layer on a PEC ground plane.

$$\frac{\eta_0}{2}J_x^e+\frac{1}{2}J_y^m=E_0. \tag{B2}$$

The magnetic surface-current density is related to the total magnetic field induced in the magnetic sheet as in Eq. (81). The total magnetic field is created by the induced currents only (the external magnetic field is zero), which allows us to write

$$J_y^m=\eta_0 H_{\rm tot}=\eta_0\left(-\frac{1}{2}J_x^e-\frac{1}{2\eta_0}J_y^m\right). \tag{B3}$$

This result defines the relation between the induced electric and magnetic surface-current densities:

$$J_y^m=-\frac{\eta_0}{3}J_x^e. \tag{B4}$$

Next, by using Eqs. (B2) and (B4), the induced averaged electric- and magnetic-current densities per unit area of the structure can be found:

$$J_x^e=\frac{3}{2\eta_0}E_0,\qquad J_y^m=-\frac{1}{2}E_0, \tag{B5}$$

and the respective induced surface-averaged electric and magnetic moments read

$$p_x=\frac{J_x^e}{j\omega}=\frac{3}{j2\omega\eta_0}E_0,\quad m_y=\frac{J_y^m}{j\omega}=-\frac{1}{j2\omega}E_0. \tag{B6}$$

Now we can find the electric and magnetic polarizabilities simply by dividing the moments by the amplitude of the incident field:

$$\eta_0\hat{\alpha}_{ee}=\frac{3}{j2\omega},\qquad \hat{\alpha}_{me}=-\frac{1}{j2\omega}. \tag{B7}$$

Similarly, we can excite the structure with a uniform magnetic field while the external electric field is set to be zero at the position of the structure and find the respective polarizabilities, writing

$$p_x=-\hat{\alpha}_{em}H_0,\qquad m_y=\hat{\alpha}_{mm}H_0. \tag{B8}$$

To satisfy the boundary condition at the PEC surface, the fields created by the two induced current sheets must cancel each other:

$$J_y^m=\eta_0 J_x^e. \tag{B9}$$

Instead of Eq. (B3), we have (the external magnetic field is not zero in this excitation scenario)

$$J_y^m=\eta_0 H_{\rm tot}=\eta_0\left(-\frac{1}{2}J_x^e-\frac{1}{2\eta_0}J_y^m+H_0\right). \tag{B10}$$

By using Eqs. (B9) and (B10), the induced electric and magnetic currents and the respective polarizabilities are found:

$$J_x^e=\frac{1}{2}H_0,\qquad J_y^m=\frac{\eta_0}{2}H_0, \tag{B11}$$

$$\hat{\alpha}_{em}=-\frac{1}{j2\omega},\qquad \frac{1}{\eta_0}\hat{\alpha}_{mm}=\frac{1}{j2\omega}. \tag{B12}$$

Thus, the effective polarizabilities per unit area of the structure read

$$\eta_0\hat{\alpha}_{ee}=\frac{3}{j2\omega},\quad \hat{\alpha}_{me}=\hat{\alpha}_{em}=-\frac{1}{j2\omega},\quad \frac{1}{\eta_0}\hat{\alpha}_{mm}=\frac{1}{j2\omega}, \tag{B13}$$

which are the required polarizabilities for perfect absorption in all thin asymmetric absorbers with a reflector at the back [Eqs. (46)–(48)].

APPENDIX C: DALLENBACH ABSORBERS AS BIANISOTROPIC HUYGENS LAYERS

Here we show that close to its operational frequency a thin Dallenbach absorber response is equivalent to that of a lossy capacitive grid separated by a free-space gap from the ground plane (high-impedance surface absorber). This equivalence is illustrated by Fig. 16. For the proof, it is important that the gap in Fig. 16(b) is optically thin, whereas the dielectric in Fig. 16(a) has the relative permittivity ϵ_r of a large absolute value which makes the gap rather optically substantial in terms of the wavelength in the dielectric medium (quarter-wavelength thickness corresponds to the thinnest Dallenbach absorber). We show that the effect of the high complex permittivity slab can be replaced by the action of a lossy grid whose reactance in the vicinity of the operation frequency is capacitive. In other words, we show the equivalence of the fundamental operation principles of the Dallenbach and the mushroom-type absorbers.

First, let us show the equivalence of their surface impedances (admittances). The surface impedance of the dielectric Dallenbach absorber is equal to (see, e.g., Ref. [4])

$$Z_D = j\eta_0 \frac{\tan kd}{\sqrt{\epsilon_r}}, \tag{C1}$$

where d is the dielectric layer thickness and k is the wave number in the dielectric $k = k' - j\alpha = k_0\sqrt{\epsilon_r}$. The complex permittivity of the layer can be expressed through the loss tangent $\epsilon_r = \epsilon_r' - j\epsilon_r'' = \epsilon_r'(1 - j\tan\delta)$. The thinnest Dallenbach absorber is described by the following equations [123]:

$$\epsilon_r' = \cos\delta \frac{\cosh(\Theta s) - \cosh(\Theta)}{\cosh(\Theta s) + \cosh(\Theta)}, \qquad \Theta = \frac{\pi}{1 - s^2}, \tag{C2}$$

where it is denoted $\Theta = 2k'd$ and $s = \tan(\delta/2)$. These equations in the absence of magnetic properties of the dielectric have a solution within the region $s < 0.25$, when the second equation (C2) practically results in the well-known condition of the quarter-wavelength thickness $2k'd \approx \pi$. Since $|\epsilon_r| \gg 1$, the smallness of dielectric losses and the quarter-wavelength restriction for d imply the inequality $\alpha d \ll 1$. By using the standard formula

$$\tan(x - jy) = \frac{\sin(2x) - j\sinh(2y)}{\cos(2x) + \cosh(2y)} \tag{C3}$$

and the quarter-wavelength condition for d, the surface admittance of a thin dielectric Dallenbach absorber [Eq. (C1)] can be approximately written in the form:

$$Y_D \equiv \frac{1}{Z_D} \approx \frac{[(\pi/2 - j\alpha d)(\cosh(2\alpha d) - 1]}{\eta_0 k_0 d \sinh(2\alpha d)}. \tag{C4}$$

Using the condition $\alpha d \ll 1$, we can write $\cosh(2\alpha d) - 1 \approx 2(\alpha d)^2$ and $\sinh(2\alpha d) \approx 2\alpha d$, reducing Eq. (C4) to

$$Y_D \approx \frac{\pi\alpha}{2k_0\eta_0} - j\frac{\alpha^2 d}{k_0\eta_0}. \tag{C5}$$

Under the condition $\alpha \approx (2k_0/\pi)$, which can be written also as $\epsilon_r'' \approx (4/\pi)$ or as $\delta \approx (4/\pi\epsilon_r')$, we obtain the equation of the approximate impedance matching on top of the absorbing surface:

$$Y_D = \frac{1}{Z_D} \approx \frac{1}{\eta_0}(1 - j\xi), \tag{C6}$$

where it is denoted $\xi = (4k_0 d/\pi) < 1$. This known result corresponds to the thinnest Dallenbach absorber and practically requires $\epsilon_r' > 15$–16 so that the absorption coefficient may exceed 0.9 [123]. From Eq. (C6), it follows that the frequency of the maximal absorption is redshifted with respect to the resonance of the surface impedance [at this resonance $Z_D = \mathrm{Re}(Z_D) \gg \eta_0$].

The surface admittance Y_{ma} of the effective mushroom absorber depicted in Fig. 16(b) is the sum of the grid admittance Y_g of a presumably capacitive grid and the input admittance of the metal-backed gap:

$$Y_{\mathrm{ma}} = Y_g + \frac{1}{j\eta_0 \tan(k_0 d)} \approx Y_g + \frac{1}{j\eta_0 k_0 d}. \tag{C7}$$

Equating admittances (C6) and (C7), we obtain

$$Y_g \approx \frac{1}{\eta_0}\left(1 + \frac{j}{k_0 d} - j\xi\right). \tag{C8}$$

In the reactive part of the grid admittance, one can neglect the small term ξ and present Eq. (C8) in the form

$$Y_g = G + j\omega C, \qquad G \approx \frac{1}{\eta_0}, \qquad C \approx \frac{2}{\omega\eta_0\pi}. \tag{C9}$$

The frequency dispersion of the effective capacitance C in the vicinity of the absorption frequency does not violate any physical requirements. What is really important is the positive sign of the imaginary part of Y_g that indicates the capacitive response of the equivalent grid, whereas the positive sign of G corresponds to absorption.

We see that the surface impedance of the Dallenbach absorber is indeed equivalent to that of a mushroom absorber with lossy and dispersive patches. The scheme of a mushroom absorber with lossy (and consequently more or less dispersive) patches was first published probably in Ref. [27] and later theoretically and experimentally developed in Refs. [11,19,106,140], and many others. For the equivalent scheme of the Dallenbach absorber it is not essential that the gap in Fig. 16(b) is filled with free space and that it has the same thickness d as the actual absorber. In our model, we can fill the gap of the equivalent absorber with a low-permittivity dielectric layer and simultaneously reduce its equivalent height that will slightly change the effective grid capacitance compared to expressions (C9).

However, the equivalence of the surface impedances even within a nonzero range of frequencies around that of the maximal absorption does not guarantee the equivalence of the electromagnetic responses of the Dallenbach and mushroom absorbers. To prove that the Dallenbach absorber is fully within our general scheme of electromagnetic absorption in thin structures, we will derive the condition of the total absorbance in terms of balanced electric **p** and magnetic **m** moments per unit area, like it was done in Appendixes A and B for other thin absorbers.

To do that, we locate the coordinate origin at the central plane of the absorber as is shown in Fig. 16(a). Then the ground plane is at $z = -d/2$ and the upper surface is at $z = d/2$, and the effective moments **p** and **m** refer to the plane $z = 0$. Let the electric field be polarized along the x axis and the magnetic field along y. Let us show that the Huygens' scatterer condition is satisfied in the regime of full absorption, i.e., that for the normal plane-wave

incidence we have $m_y = \eta_0 p_x$. Also, as was done in Appendix A, we combine this proof with the demonstration of the effective bianisotropy of the absorber. In other words, we show that both mushroom and Dallenbach absorbers turn out to be equivalent to an array of omega particles, which means the equivalence of their electromagnetic response to a plane wave.

For this proof, we derive the effective polarizabilities defined with respect to the local fields: $\alpha_{ee} = p_x/E_x^{\rm loc}$, $\alpha_{mm} = m_y/H_y^{\rm loc}$, $\alpha_{em} = p_x/H_y^{\rm loc} = -j\Omega$, and $\alpha_{me} = m_y/E_x^{\rm loc} = j\Omega$. Here Ω is the magnetoelectric coefficient of an effective omega particle modeling the unit area of the Dallenbach absorber. To model the local fields, we again use the standing-wave approach of Appendix A, Fig. 19. For the electric excitation of the Dallenbach absorber shown in Fig. 16(a), the external fields in our model are equal to

$$E_x^{\rm ext}(z) = 2E_0\cos(k_0 z), \qquad H_y^{\rm ext}(z) = 2E_0\sin(k_0 z)/\eta_0; \tag{C10}$$

i.e., the local fields are as follows:

$$E_x^{\rm loc} \equiv E_x^{\rm ext}(0) = 2E_0, \qquad H_y^{\rm loc} \equiv H_y^{\rm ext}(0) = 0. \tag{C11}$$

For the magnetic excitation, the external fields are equal to

$$H_y^{\rm ext}(z) = 2E_0\cos(k_0 z)/\eta_0, \qquad E_x^{\rm ext}(z) = 2E_0\sin(k_0 z), \tag{C12}$$

whereas the local fields are as follows:

$$H_y^{\rm loc} \equiv H_y^{\rm ext}(0) = 2E_0/\eta_0, \qquad E_x^{\rm loc} \equiv E_x^{\rm ext}(0) = 0. \tag{C13}$$

First, consider the electric excitation described by Eq. (C10). Let $\mathbf{E}_P(z) = E_P(z)\mathbf{x}_0$ and $\mathbf{H}_P(z) = H_P(z)\mathbf{y}_0$, respectively, denote the electric and magnetic fields produced by the bulk polarization $\mathbf{P}(z) = P(z)\mathbf{x}_0$ of the dielectric layer. Denoting $\mathbf{J}_{\rm met} = J_{\rm met}\mathbf{y}_0$ the amplitude of the surface current induced on the metal plane, we can write the boundary condition at the upper interface of the absorber:

$$2E_0\cos\left(\frac{k_0 d}{2}\right) + E_P\left(\frac{d}{2}\right) - \frac{\eta_0 J_{\rm met}}{2}e^{-jk_0 d} = Z_D\frac{2E_0\sin(\frac{k_0 d}{2}) + H_P(\frac{d}{2}) - \frac{J_{\rm met}}{2}e^{-jk_0 d}}{\eta_0}. \tag{C14}$$

Here the left-hand part of Eq. (C14) is the total electric field $\mathbf{E} = E\mathbf{x}_0$ on top of the structure, at $z = d/2$. The right-hand side is the product of the surface impedance of the Dallenbach absorber by the total magnetic field $\mathbf{H} = H\mathbf{y}_0$ on top of it. The total electric field comprises even and odd parts and inside the structure can be searched in the form

$$E(z) = A\sin kz + B\cos kz. \tag{C15}$$

Coefficients A and B are related by the PEC boundary condition at $z = -d/2$:

$$-A\sin\left(\frac{kd}{2}\right) + B\cos\left(\frac{kd}{2}\right) = 0. \tag{C16}$$

In the absorption regime $kd = \pi/2 - j\alpha d$, where $\alpha d \ll 1$. In these derivations we adopt an approximation $kd \approx \pi/2$. Then Eq. (C16) results in $B = A$.

In Eq. (C14), the magnetic field H_P is equal $H_P = E_P/\eta_0$, and it is possible to express $E_P(d/2)$ through the unknown constant A. To do that, we split the dielectric layer d to elementary layers dz and present the field E_P as the integral of partial fields created by elementary current sheets $dJ_P(z) = j\omega P(z)dz$, where $P(z) = \epsilon_0(\epsilon_r - 1)E(z)$:

$$E_P\left(\pm\frac{d}{2}\right) = \frac{jk_0(\epsilon_r - 1)}{2}\int_{-d/2}^{d/2} E(z)e^{-jk_0[(d/2)\mp z]}dz. \tag{C17}$$

Substitution of Eq. (C15) with $B = A$ yields Eq. (C17) to

$$E_P\left(\pm\frac{d}{2}\right) = \frac{jk_0 A(\epsilon_r - 1)}{2} \times \int_{-d/2}^{d/2} e^{-jk_0[(d/2)\mp z]}(\sin kz + \cos kz)dz. \tag{C18}$$

The value $E_P(\pm d/2)$ after integration of Eq. (C18) should be substituted into Eq. (C14). This substitution gives us the first equation relating constants A and $J_{\rm met}$. The second equation is the equivalence of $E(d/2)$ corresponding to the left-hand side of Eq. (C14) and $E(d/2)$ corresponding to the right-hand side of Eq. (C15):

$$2E_0\cos\left(\frac{k_0 d}{2}\right) + E_P\left(\frac{d}{2}\right) - \frac{\eta_0 J_{\rm met}}{2}e^{-jk_0 d} = A\left[\sin\left(\frac{kd}{2}\right) + \cos\left(\frac{kd}{2}\right)\right]. \tag{C19}$$

To calculate the integral in Eq. (C18), we used the condition of the optically thin layer $k_0 d \ll 1$:

$$e^{-jk_0[(d/2)\mp z]} \approx 1 - jk_0\left(\frac{d}{2} \mp z\right), \quad \text{if } |z| \le \frac{d}{2}.$$

Then Eq. (C18) can be reduced to the following known integrals:

$$\int \left\{ \begin{matrix} \sin x \\ \cos x \end{matrix} \right\} dx = \left\{ \begin{matrix} -\cos x \\ \sin x \end{matrix} \right\},$$
$$\int x \left\{ \begin{matrix} \sin x \\ \cos x \end{matrix} \right\} dx = \left\{ \begin{matrix} \sin x \\ \cos x \end{matrix} \right\} \mp x \times \left\{ \begin{matrix} \cos x \\ \sin x \end{matrix} \right\}. \quad \text{(C20)}$$

Finally, we obtain for the integral in Eq. (C18):

$$\int_{-d/2}^{d/2} e^{-jk_0[(d/2)\mp z]}(\sin kz + \cos kz)dz \approx \frac{2jk_0 d}{k}\cos\left(\frac{kd}{2}\right) + \frac{2(1 \mp jk_0 d)}{k}\sin\left(\frac{kd}{2}\right). \quad \text{(C21)}$$

Substituting Eqs. (C18) and (C21) into the left-hand side of Eq. (C14) and using approximations $\exp(-jk_0 d) \approx 1 - jk_0 d$ and $\cos(k_0 d/2) \approx 1$, we obtain

$$E\left(\frac{d}{2}\right) = 2E_0 + \frac{jk_0 A(\epsilon_r - 1)}{k} \times \left[jk_0 d \sin\frac{kd}{2} + (1 - jk_0 d)\cos\frac{kd}{2}\right] - \frac{J_{\text{met}}\eta_0}{2}(1 - jk_0 d). \quad \text{(C22)}$$

The expression for $H(d/2)$ in the right-hand side of Eq. (C14) being multiplied by η_0 differs from Eq. (C22) only by the first term, expressing the external magnetic field:

$$\eta_0 H\left(\frac{d}{2}\right) = k_0 d E_0 + \frac{jk_0 A(\epsilon_r - 1)}{k} \times \left[jk_0 d \sin\frac{kd}{2} + (1 - jk_0 d)\cos\frac{kd}{2}\right] + \frac{J_{\text{met}}\eta_0}{2}(1 - jk_0 d). \quad \text{(C23)}$$

Using Eqs. (C22) and (C23) and taking into account that in the absorption regime $\cos(kd/2) \approx \sin(kd/2) \approx 1/\sqrt{2}$, we can rewrite Eq. (C14) after simple algebra in the form

$$\frac{J_{\text{met}}\eta_0}{2}(1 - jk_0 d) + \frac{\sqrt{2}k_0 d(\epsilon_r - 1)}{\pi}A = \left(1 - \frac{k_0 d Z_D}{\eta_0}\right)\frac{2E_0}{1 - \frac{Z_D}{\eta_0}}. \quad \text{(C24)}$$

The second condition—Eq. (C19)—after the same substitutions takes the form

$$2E_0 - \frac{J_{\text{met}}\eta_0}{2}(1 - jk_0 d) - \frac{\sqrt{2}k_0 d(\epsilon_r - 1)}{\pi}A[k_0 d - j(1 - jk_0 d)] = \sqrt{2}A. \quad \text{(C25)}$$

The solution for J_{met} can be written in the form

$$J_{\text{met}} = \Psi A, \qquad \Psi = \frac{2\sqrt{2}(F-1)}{\eta_0(1 - jk_0 d)}, \qquad F = \frac{k_0 d(\epsilon_r - 1)}{\pi}, \quad \text{(C26)}$$

and for A we obtain

$$A = \Phi E_0, \qquad \Phi = \frac{\sqrt{2}(1 - \frac{k_0 d Z_D}{\eta_0})}{(1 - \frac{Z_D}{\eta_0})}. \quad \text{(C27)}$$

Following to Eq. (C6), in the vicinity of the frequency of total absorption $1 - (Z_D/\eta_0) \approx -j\xi$, where $\xi \ll 1$. Therefore,

$$\Phi \approx \frac{\sqrt{2}j[1 - k_0 d(1 - j\xi)]}{\xi}. \quad \text{(C28)}$$

Notice that the calculation of $E_P(-d/2)$ using Eq. (C18) allowed a useful check of our derivations. We have checked that the equation

$$2E_0 \cos\left(\frac{k_0 d}{2}\right) + E_P\left(-\frac{d}{2}\right) - J_{\text{met}}\frac{\eta_0}{2} = 0 \quad \text{(C29)}$$

is identically satisfied with Eqs. (C26) and (C28).

After finding the two relevant constants A and J_{met}, we can determine the effective polarizabilities referring to the unit surface area. From the general definitions of electric and magnetic dipole moments, it follows that

$$p_x = \int_{-d/2}^{d/2} P(z)dz + \frac{J_{\text{met}}}{j\omega}, \qquad m_y = \frac{j\omega\mu_0}{2}\int_{-d/2}^{d/2} zP(z)dz - \frac{\mu_0 d J_{\text{met}}}{2}. \quad \text{(C30)}$$

Substituting formula $P(z) = \epsilon_0(\epsilon_r - 1)A(\sin kz + \cos kz)$ into Eq. (C30), we again come to known integrals (C20) and using the quarter-wavelength condition $kd \approx \pi/2$ obtain

$$p_x \approx \frac{2\sqrt{2}E_0 A}{\omega\eta_0}\left[F - \frac{1 - F}{1 - jk_0 d}\right] \quad \text{(C31)}$$

and

$$m_y \approx \frac{-jk_0 d\sqrt{2}E_0 A}{\omega}\left[F + \frac{1-F}{1-jk_0 d}\right]. \tag{C32}$$

In accordance to the definitions of the effective polarizabilities and using Eqs. (C11) and (C13), we can rewrite Eqs. (C31) and (C32) as follows:

$$\alpha_{ee} \approx \frac{2j[1-k_0 d(1-j\xi)]}{\xi\omega\eta_0}\left(F - \frac{1-F}{1-jk_0 d}\right), \tag{C33}$$

$$\alpha_{me} \approx \frac{k_0 d[1-k_0 d(1-j\xi)]}{\xi\omega}\left(F + \frac{1-F}{1-jk_0 d}\right). \tag{C34}$$

Since in our derivations we neglected the terms of the order of $(k_0 d)^2$, Eqs. (C33) and (C34) should be simplified neglecting quadratic terms in them:

$$\alpha_{ee} \approx \frac{2j}{\xi\omega\eta_0}\frac{[F(2-jk_0 d)-1]}{1-jk_0 d}, \qquad \alpha_{me} \approx \frac{k_0 d}{\xi\omega(1-jk_0 d)}. \tag{C35}$$

Formulas (C35) are self-consistent within our first-order model.

Next, let us consider the magnetic excitation given by Eq. (C12). On the top surface of the absorber, we have the boundary condition:

$$2E_0 \sin\left(\frac{k_0 d}{2}\right) + E_P\left(\frac{d}{2}\right) - \frac{\eta_0 J_{\text{met}}}{2} e^{-jk_0 d} = Z_D \frac{2E_0 \cos(\frac{k_0 d}{2}) + H_P(\frac{d}{2}) - \frac{J_{\text{met}}}{2} e^{-jk_0 d}}{\eta_0}. \tag{C36}$$

Again, the dielectric layer d is polarized electrically and its bulk polarization $P(z)$ is still equal to $\epsilon_0(\epsilon_r - 1)E(z)$, where the total electric field inside the layer has the form $E(z) = A' \sin kz + B' \cos kz$. The field produced by the polarized dielectric layer is still expressed by Eq. (C17). Again, the PEC boundary condition at $z = -(d/2)$ together with the absorption condition $kd \approx \pi/2$ results in the equivalence $B' = A'$. An interesting fact that the electric excitation and magnetic excitation result in the same distribution of the total field across the absorber is the peculiarity of the thinnest Dallenbach absorption: For any distribution of the external electromagnetic field across it, the electric and magnetic fields are distributed in it in the same form: $E(z) \sim \cos kz + \sin kz$ and $H(z) \sim \cos kz - \sin kz$.

Further derivations practically repeat the same steps as above, and we obtain for the magnetic excitation of the absorber the following formulas for the effective polarizabilities:

$$\alpha_{mm} \approx \frac{2j\eta_0[1-k_0 d(1-j\xi)]}{\xi\omega}\left[\frac{F}{1-jk_0 d} - (1-F)\right], \tag{C37}$$

$$\alpha_{em} \approx -\frac{k_0 d[1-k_0 d(1-j\xi)]}{\xi\omega}\left[\frac{F}{1-jk_0 d} + (1-F)\right]. \tag{C38}$$

For self-consistency of the model, we should neglect the second-order terms in these relations, which gives

$$\alpha_{mm} = \frac{2j\eta_0[F(2-jk_0 d)-1+jk_0 d]}{\xi\omega(1-jk_0 d)}, \qquad \alpha_{em} = -a_{me} = -\frac{k_0 d}{\xi\omega(1-jk_0 d)}. \tag{C39}$$

Now let a plane wave be normally incident on a Dallenbach absorber. Then we have for the induced magnetic and electric dipole moments per unit area

$$p_x = \alpha_{ee}E_0 + \alpha_{em}H_0 = E_0\left(\alpha_{ee} + \frac{\alpha_{em}}{\eta_0}\right), \tag{C40}$$

$$m_y = \alpha_{em}E_0 + \alpha_{mm}H_0 = E_0\left(-\alpha_{em} + \frac{\alpha_{mm}}{\eta_0}\right). \tag{C41}$$

These equations after substitutions of Eqs. (C35) and (C39) become

$$p_x = \frac{2jE_0}{\xi\omega\eta_0}\frac{[F(2-jk_0 d)-1+\frac{jk_0 d}{2}]}{(1-jk_0 d)}, \qquad m_y = \frac{2jE_0}{\xi\omega}\frac{[-\frac{jk_0 d}{2}+F(2-jk_0 d)-1+jk_0 d]}{(1-jk_0 d)}. \tag{C42}$$

Equations (C42) show that the condition of the Huygens scatterer $m_y = \eta_0 p_x$ is fulfilled. The thin Dallenbach absorber is fully within our general scheme.

[1] W. Dallenbach and W. Kleinsteuber, Reflection and absorption of decimeter-waves by plane dielectric layers, Hochfrequenztechnik und Elektroakustik **51**, 152 (1938).

[2] W. W. Salisbury, Absorbent body of electromagnetic waves, U.S. Patent No. 2,599,944, 10 June 1952.

[3] E. F. Knott, J. F. Shaeffer, and M. T. Tuley, *Radar Cross Section* (Artech House, London, 1993).

[4] B. A. Munk, *Frequency Selective Surfaces: Theory and Design* (Wiley, New York, 2000).

[5] A. Serdyukov, I. Semchenko, S. Tretyakov, and A. Sihvola, *Electromagnetics of Bi-anisotropic Materials: Theory and Applications* (Gordon and Breach, Amsterdam, 2001).

[6] R. L. Fante and M. T. McCormack, Reflection properties of the Salisbury screen, IEEE Trans. Antennas Propag. **36**, 1443 (1988).

[7] N. Liu, M. Mesch, T. Weiss, M. Hentschel, and H. Giessen, Infrared perfect absorber and its application as plasmonic sensor, Nano Lett. **10**, 2342 (2010).

[8] J. Grant, Y. Ma, S. Saha, L. B. Lok, A. Khalid, and D. R. S. Cumming, Polarization insensitive terahertz metamaterial absorber, Opt. Lett. **36**, 1524 (2011).

[9] H. A. Atwater and A. Polman, Plasmonics for improved photovoltaic devices, Nat. Mater. **9**, 205 (2010).

[10] M. Laroche, R. Carminati, and J.-J. Greffet, Near-field thermophotovoltaic energy conversion, J. Appl. Phys. **100**, 063704 (2006).

[11] S. Simms and V. Fusco, Thin radar absorber using artificial magnetic ground plane, Electron. Lett. **41**, 1311 (2005).

[12] W. Padilla and X. Liu, Perfect electromagnetic absorbers from microwave to optical, SPIE Newsroom, doi:10.1117/2.1201009.003137, 2010.

[13] H. Cheng, S. Chen, H. Yang, J. Li, X. An, C. Gu, and J. Tian, A polarization insensitive and wide-angle dual-band nearly perfect absorber in the infrared regime, J. Opt. **14**, 085102 (2012).

[14] J. Hao, J. Wang, X. Liu, W. J. Padilla, L. Zhou, and M. Qiu, High performance optical absorber based on a plasmonic metamaterial, Appl. Phys. Lett. **96**, 251104 (2010).

[15] K. N. Rozanov, Ultimate thickness to bandwidth ratio of radar absorbers, IEEE Trans. Antennas Propag. **48**, 1230 (2000).

[16] C. Sohl, M. Gustafsson, and G. Kristensson, Physical limitations on metamaterials: Restrictions on scattering and absorption over a frequency interval, J. Phys. D **40**, 7146 (2007).

[17] S. A. Tretyakov, Uniaxial omega medium as a physically realizable alternative for the perfectly matched layer (PML), J. Electromagn. Waves Appl. **12**, 821 (1998).

[18] S. A. Tretyakov and T. G. Kharina, The perfectly matched layer as a synthetic material with active inclusions, Electromagnetics **20**, 155 (2000).

[19] S. A. Tretyakov and S. I. Maslovski, Thin absorbing structure for all incident angles based on the use of a high-impedance surface, Microwave Opt. Technol. Lett. **38**, 175 (2003).

[20] N. I. Landy, C. M. Bingham, T. Tyler, N. Jokerst, D. R. Smith, and W. J. Padilla, Design, theory, and measurement of a polarization-insensitive absorber for terahertz imaging, Phys. Rev. B **79**, 125104 (2009).

[21] O. Luukkonen, F. Costa, C. R. Simovski, A. Monorchio, and S. A. Tretyakov, A thin electromagnetic absorber for wide incidence angles and both polarizations, IEEE Trans. Antennas Propag. **57**, 3119 (2009).

[22] B. Zhu, Z. Wang, C. Huang, Y. Feng, J. Zhao, and T. Jiang, Polarization insensitive metamaterial absorber with wide incident angle, Prog. Electromagn. Res. **101**, 231 (2010).

[23] K. Aydin, V. E. Ferry, R. M. Briggs, and H. A. Atwater, Broadband polarization-independent resonant light absorption using ultrathin plasmonic super absorbers, Nat. Commun. **2**, 517 (2011).

[24] L. Lu, S. Qu, H. Ma, F. Yu, S. Xia, Z. Xu, and P. Bai, A polarization-independent wide-angle dual directional absorption metamaterial absorber, Prog. Electromagn. Res. M **27**, 91 (2012).

[25] M. Diem, T. Koschny, and C. M. Soukoulis, Wide-angle perfect absorber/thermal emitter in the terahertz regime, Phys. Rev. B **79**, 033101 (2009).

[26] J.-P. Berenger, A perfectly matched layer for the absorption of electromagnetic waves, J. Comput. Phys. **114**, 185 (1994).

[27] N. Engheta, in *Proceedings of the IEEE International Symposium on Antennas and Propagation, 2002* (IEEE, New York, 2002), Vol. 2, p. 392.

[28] F. Bilotti, A. Toscano, K. B. Alici, E. Ozbay, and L. Vegni, Design of miniaturized narrowband absorbers based on resonant-magnetic inclusions, IEEE Trans. Electromagn. Compat. **53**, 63 (2011).

[29] N. I. Landy, S. Sajuyigbe, J. J. Mock, D. R. Smith, and W. J. Padilla, Perfect Metamaterial Absorber, Phys. Rev. Lett. **100**, 207402 (2008).

[30] V. T. Pham, J. W. Park, D. L. Vu, H. Y. Zheng, J. Y. Rhee, K. W. Kim, and Y. P. Lee, THz-metamaterial absorbers, Adv. Nat. Sci. Nanosci. Nanotechnol. **4**, 015001 (2013).

[31] G. Dayal and S. A. Ramakrishna, Design of highly absorbing metamaterials for infrared frequencies, Opt. Express **20**, 17503 (2012).

[32] C. M. Watts, X. Liu, and W. J. Padilla, Metamaterial electromagnetic wave absorbers, Adv. Mater. **24**, OP98 (2012).

[33] T. Maier and H. Brückl, Wavelength-tunable microbolometers with metamaterial absorbers, Opt. Lett. **34**, 3012 (2009).

[34] J. Rosenberg, R. V. Shenoi, T. E. Vandervelde, S. Krishna, and O. Painter, A multispectral and polarization-selective surface-plasmon resonant midinfrared detector, Appl. Phys. Lett. **95**, 161101 (2009).

[35] E. Rephaeli and S. Fan, Absorber and emitter for solar thermo-photovoltaic systems to achieve efficiency exceeding the Shockley-Queisser limit, Opt. Express **17**, 15145 (2009).

[36] J. A. Schuller, E. S. Barnard, W. Cai, Y. C. Jun, J. S. White, and M. L. Brongersma, Plasmonics for extreme light concentration and manipulation, Nat. Mater. **9**, 193 (2010).

[37] X. Liu, T. Tyler, T. Starr, A. F. Starr, N. M. Jokerst, and W. J. Padilla, Taming the Blackbody with Infrared Metamaterials as Selective Thermal Emitters, Phys. Rev. Lett. **107**, 045901 (2011).

[38] A. Tittl, P. Mai, R. Taubert, D. Dregely, N. Liu, and H. Giessen, Palladium-based plasmonic perfect absorber in the visible wavelength range and its application to Hydrogen sensing, Nano Lett. **11**, 4366 (2011).

[39] J.-J. Greffet, Controlled incandescence, Nature (London) **478**, 191 (2011).

[40] J. N. Munday and H. A. Atwater, Large integrated absorption enhancement in plasmonic solar cells by combining metallic gratings and antireflection coatings, Nano Lett. **11**, 2195 (2011).

[41] S. A. Kuznetsov, A. G. Paulish, A. V. Gelfand, P. A. Lazorskiy, and V. N. Fedorinin, Bolometric THz-to-IR converter for terahertz imaging, Appl. Phys. Lett. **99**, 023501 (2011).

[42] C. Hägglund and S. P. Apell, Plasmonic near-field absorbers for ultrathin solar cells, J. Phys. Chem. Lett. **3**, 1275 (2012).

[43] Y. Cui, K. H. Fung, J. Xu, H. Ma, Y. Jin, S. He, and N. X. Fang, Ultrabroadband light absorption by a sawtooth anisotropic metamaterial slab, Nano Lett. **12**, 1443 (2012).

[44] F. Alves, D. Grbovic, B. Kearney, N. V. Lavrik, and G. Karunasiri, Bi-material terahertz sensors using metamaterial structures, Opt. Express **21**, 13256 (2013).

[45] F. B. P. Niesler, J. K. Gansel, S. Fischbach, and M. Wegener, Metamaterial metal-based bolometers, Appl. Phys. Lett. **100**, 203508 (2012).

[46] H. Tao, N. I. Landy, C. M. Bingham, X. Zhang, R. D. Averitt, and W. J. Padilla, A metamaterial absorber for the terahertz regime: Design, fabrication and characterization, Opt. Express **16**, 7181 (2008).

[47] H. Tao, C. M. Bingham, A. C. Strikwerda, D. Pilon, D. Shrekenhamer, N. I. Landy, K. Fan, X. Zhang, W. J. Padilla, and R. D. Averitt, Highly flexible wide angle of incidence terahertz metamaterial absorber: Design, fabrication, and characterization, Phys. Rev. B **78**, 241103 (2008).

[48] X. Liu, T. Starr, A. F. Starr, and W. J. Padilla, Infrared Spatial and Frequency Selective Metamaterial with Near-Unity Absorbance, Phys. Rev. Lett. **104**, 207403 (2010).

[49] Y. Jin, S. Xiao, N. A. Mortensen, and S. He, Arbitrarily thin metamaterial structure for perfect absorption and giant magnification, Opt. Express **19**, 11114 (2011).

[50] H.-T. Chen, J. Zhou, J. F. O'Hara, F. Chen, A. K. Azad, and A. J. Taylor, Antireflection Coating using Metamaterials and Identification of its Mechanism, Phys. Rev. Lett. **105**, 073901 (2010).

[51] H.-T. Chen, Interference theory of metamaterial perfect absorbers, Opt. Express **20**, 7165 (2012).

[52] X. Shen, Y. Yang, Y. Zang, J. Gu, J. Han, W. Zhang, and T. J. Cui, Triple-band terahertz metamaterial absorber: Design, experiment, and physical interpretation, Appl. Phys. Lett. **101**, 154102 (2012).

[53] J. Sun, L. Liu, G. Dong, and J. Zhou, An extremely broad band metamaterial absorber based on destructive interference, Opt. Express **19**, 21155 (2011).

[54] T. V. Teperik, V. V. Popov, and F. J. García de Abajo, Total light absorption in plasmonic nanostructures, J. Opt. A **9**, S458 (2007).

[55] Q.-Y. Wen, Y.-S. Xie, H.-W. Zhang, Q.-H. Yang, Y.-X. Li, and Y.-L. Liu, Transmission line model and fields analysis of metamaterial absorber in the terahertz band, Opt. Express **17**, 20256 (2009).

[56] Y.-Q. Pang, Y.-J. Zhou, and J. Wang, Equivalent circuit method analysis of the influence of frequency selective surface resistance on the frequency response of metamaterial absorbers, J. Appl. Phys. **110**, 023704 (2011).

[57] Y. Pang, H. Cheng, Y. Zhou, and J. Wang, Analysis and design of wire-based metamaterial absorbers using equivalent circuit approach, J. Appl. Phys. **113**, 114902 (2013).

[58] M. P. Hokmabadi, D. S. Wilbert, P. Kung, and S. M. Kim, Design and analysis of perfect terahertz metamaterial absorber by a novel dynamic circuit model, Opt. Express **21**, 16455 (2013).

[59] F. Costa, S. Genovesi, A. Monorchio, and G. Manara, A circuit-based model for the interpretation of perfect metamaterial absorbers, IEEE Trans. Antennas Propag. **61**, 1201 (2013).

[60] D. Y. Shchegolkov, A. K. Azad, J. F. O'Hara, and E. I. Simakov, Perfect subwavelength fishnetlike metamaterial-based film terahertz absorbers, Phys. Rev. B **82**, 205117 (2010).

[61] X.-Y. Peng, B. Wang, S. Lai, D. H. Zhang, and J.-H. Teng, Ultrathin multi-band planar metamaterial absorber based on standing wave resonances, Opt. Express **20**, 27756 (2012).

[62] J. Zhou, H.-T. Chen, T. Koschny, A. K. Azad, A. J. Taylor, C. M. Soukoulis, and J. F. O'Hara, Application of metasurface description for multilayered metamaterials and an alternative theory for metamaterial perfect absorber, arXiv:1111.0343.

[63] H. Y. Zheng, X. R. Jin, J. W. Park, Y. H. Lu, J. Y. Rhee, W. H. Jang, H. Cheong, and Y. P. Lee, Tunable dual-band perfect absorbers based on extraordinary optical transmission and Fabry-Perot cavity resonance, Opt. Express **20**, 24002 (2012).

[64] M. K. Hedayati, M. Javaherirahim, B. Mozooni, R. Abdelaziz, A. Tavassolizadeh, V. S. K. Chakravadhanula, V. Zaporojtchenko, T. Strunkus, F. Faupel, and M. Elbahri, Design of a perfect black absorber at visible frequencies using plasmonic metamaterials, Adv. Mater. **23**, 5410 (2011).

[65] Y. Zeng, H.-T. Chen, and D. A. R. Dalvit, The role of magnetic dipoles and non-zero-order Bragg waves in metamaterial perfect absorbers, Opt. Express **21**, 3540 (2013).

[66] J. W. Park, P. V. Tuong, J. Y. Rhee, K. W. Kim, W. H. Jang, E. H. Choi, L. Y. Chen, and Y. P. Lee, Multi-band metamaterial absorber based on the arrangement of donut-type resonators, Opt. Express **21**, 9691 (2013).

[67] Y. Ra'di, V. S. Asadchy, and S. A. Tretyakov, Total absorption of electromagnetic waves in ultimately thin layers, IEEE Trans. Antennas Propag. **61**, 4606 (2013).

[68] D. Pozar, Scattered and absorbed powers in receiving antennas, IEEE Antennas Propag. Mag. **46**, 144 (2004).

[69] S. Tretyakov, *Analytical Modeling in Applied Electromagnetics* (Artech, Norwood, MA, 2003).

[70] J. R. Tischler, M. S. Bradley, and V. Bulović, Critically coupled resonators in vertical geometry using a planar mirror and a 5 nm thick absorbing film, Opt. Lett. **31**, 2045 (2006).

[71] J. R. Tischler, M. S. Bradley, Q. Zhang, T. Atay, A. Nurmikko, and V. Bulović, Solid state cavity QED: Strong coupling in organic thin films, Org. Electron. **8**, 94 (2007).

[72] S. D. Gupta, Strong-interaction-mediated critical coupling at two distinct frequencies, Opt. Lett. **32**, 1483 (2007).

[73] S. Deb, S. Dutta-Gupta, J. Banerji, and S. Dutta Gupta, Critical coupling at oblique incidence, J. Opt. A **9**, 555 (2007).

[74] Y. Xiang, X. Dai, J. Guo, H. Zhang, S. Wen, and D. Tang, Critical coupling with graphene-based hyperbolic metamaterials, Sci. Rep. **4**, 5483 (2014).

[75] S. Ramo and J. R. Whinnery, *Fields and Waves in Modern Radio* (Wiley, New York, 1944).

[76] W. Wan, Y. Chong, L. Ge, H. Noh, A. D. Stone, and H. Cao, Time-reversed lasing and interferometric control of absorption, Science **331**, 889 (2011).

[77] V. Klimov, S. Sun, and G.-Y. Guo, Coherent perfect nanoabsorbers based on negative refraction, Opt. Express **20**, 13071 (2012).

[78] S. Longhi, Coherent perfect absorption in a homogeneously broadened two-level medium, Phys. Rev. A **83**, 055804 (2011).

[79] S. Longhi, $\mathcal{PT}$-symmetric laser absorber, Phys. Rev. A **82**, 031801 (2010).

[80] G. Pirruccio, L. M. Moreno, G. Lozano, and J. G. Rivas, Coherent and broadband enhanced optical absorption in graphene, ACS Nano **7**, 4810 (2013).

[81] Y. D. Chong, L. Ge, H. Cao, and A. D. Stone, Coherent Perfect Absorbers: Time-Reversed Lasers, Phys. Rev. Lett. **105**, 053901 (2010).

[82] D. A. B. Miller, On perfect cloaking, Opt. Express **14**, 12457 (2006).

[83] M. Selvanayagam and G. V. Eleftheriades, Experimental Demonstration of Active Electromagnetic Cloaking, Phys. Rev. X **3**, 041011 (2013).

[84] T. Niemi, A. O. Karilainen, and S. A. Tretyakov, Synthesis of polarization transformers, IEEE Trans. Antennas Propag. **61**, 3102 (2013).

[85] V. K. Varadan, V. V. Varadan, and A. Lakhtakia, On the possibility of designing anti-reflection coating using chiral composites, J. Wave-Mater. Interact. **2**, 71 (1987).

[86] D. L. Jaggard and N. Engheta, Chirosorb^{TM} as an invisible medium, Electron. Lett. **25**, 173 (1989).

[87] S. A. Tretyakov, A. A. Sochava, and C. R. Simovski, Influence of chiral shapes of individual inclusions on the absorption in chiral composite coatings, Electromagnetics **16**, 113 (1996).

[88] D. M. Pozar, *Microwave Engineering* (Wiley, New York, 2012).

[89] J. Vehmas, S. Hrabar, and S. Tretyakov, Omega transmission lines with applications to effective medium models of metamaterials, J. Appl. Phys. **115**, 134905 (2014).

[90] V. Asadchy, I. Faniayeu, Y. Ra'di, I. Semchenko, and S. Khakhomov, in *Proceedings of the 7th International Congress on Advanced Electromagnetic Materials in Microwaves and Optics—Metamaterials, Bordeaux, France, 2013* (IEEE, New York, USA, 2013), p. 244.

[91] I. Faniayeu, V. Asadchy, T. Dziarzhauskaya, I. Semchenko, and S. Khakhomov, A single-layer meta-atom absorber, arXiv:1404.1816.

[92] S. Gu, J. P. Barrett, T. H. Hand, B.-I. Popa, and S. A. Cummer, A broadband low-reflection metamaterial absorber, J. Appl. Phys. **108**, 064913 (2010).

[93] C. A. Valagiannopoulos and S. A. Tretyakov, Symmetric absorbers realized as gratings of PEC cylinders covered by ordinary dielectrics, IEEE Trans. Antennas Propag. **62**, 5089 (2014).

[94] S. A. Tretyakov, C. R. Simovski, and A. A. Sochava, in *Advances in Complex Electromagnetic Materials*, edited by A. Priou, A. Sihvola, S. Tretyakov, and A. Vinogradov (Kluwer Academic, Dordrecht, 1997), pp. 271–280.

[95] C. Hu, X. Li, Q. Feng, X. Chen, and X. Luo, Introducing dipole-like resonance into magnetic resonance to realize simultaneous drop in transmission and reflection at terahertz frequency, J. Appl. Phys. **108**, 053103 (2010).

[96] Y. Cheng, H. Yang, Z. Cheng, and B. Xiao, A planar polarization-insensitive metamaterial absorber, Photonics Nanostruct. Fundam. Appl. **9**, 8 (2011).

[97] F. Costa, S. Genovesi, and A. Monorchio, On the bandwidth of high-impedance frequency selective surfaces, IEEE Antennas Wireless Propag. Lett. **8**, 1341 (2009).

[98] H. Greve, C. Pochstein, H. Takele, V. Zaporojtchenko, F. Faupel, A. Gerber, M. Frommberger, and E. Quandt, Nanostructured magnetic Fe-Ni-Co/Teflon multilayers for high-frequency applications in the gigahertz range, Appl. Phys. Lett. **89**, 242501 (2006).

[99] I. T. Iakubov, A. N. Lagarkov, S. A. Maklakov, A. V. Osipov, K. N. Rozanov, I. A. Ryzhikov, V. V. Samsonova, and A. O. Sboychakov, Microwave and static magnetic properties of multi-layered iron-based films, J. Magn. Magn. Mater. **321**, 726 (2009).

[100] L. B. Kong, Z. W. Li, L. Liu, R. Huang, M. Abshinova, Z. H. Yang, C. B. Tang, P. K. Tan, C. R. Deng, and S. Matitsine, Recent progress in some composite materials and structures for specific electromagnetic applications, Int. Mater. Rev. **58**, 203 (2013).

[101] O. Acher, Copper vs. iron: Microwave magnetism in the metamaterial age, J. Magn. Magn. Mater. **321**, 2093 (2009).

[102] P. Ikonen, S. I. Maslovski, C. R. Simovski, and S. A. Tretyakov, On artificial magnetodielectric loading for improving the impedance bandwidth properties of microstrip antennas, IEEE Trans. Antennas Propag. **54**, 1654 (2006).

[103] D. Sievenpiper, L. Zhang, R. F. J. Broas, N. G. Alexópolous, and E. Yablonovitch, High-impedance electromagnetic surfaces with a forbidden frequency band, IEEE Trans. Microw. Theory Tech. **47**, 2059 (1999).

[104] S. A. Tretyakov and C. R. Simovski, Dynamic model of artificial reactive impedance surfaces, J. Electromagn. Waves Appl. **17**, 131 (2003).

[105] O. Luukkonen, C. Simovski, G. Granet, G. Goussetis, D. Lioubtchenko, A. V. Räisänen, and S. A. Tretyakov, Simple and accurate analytical model of planar grids and high-impedance surfaces comprising metal strips or patches, IEEE Trans. Antennas Propag. **56**, 1624 (2008); **58**, 2162(E) (2010).

[106] Y. Okano, S. Ogino, and K. Ishikawa, Development of optically transparent ultrathin microwave absorber for ultrahigh-frequency RF identification system, IEEE Trans. Microw. Theory Tech. **60**, 2456 (2012).

[107] F. Terracher and G. Berginc, A broadband dielectric microwave absorber with periodic metallizations, J. Electromagn. Waves Appl. **13**, 1725 (1999).

[108] A. N. Lagarkov, V. N. Semenenko, V. A. Chistyaev, D. E. Ryabov, S. A. Tretyakov, and C. R. Simovski, Resonance properties of bi-helix media at microwaves, Electromagnetics **17**, 213 (1997).

[109] J. B. Pendry, A. J. Holden, D. J. Robbins, and W. J. Stewart, Magnetism from conductors and enhanced nonlinear phenomena, IEEE Trans. Microw. Theory Techn. **47**, 2075 (1999).

[110] J. Hao, V. Sadaune, L. Burgnies, and D. Lippens, Ferroelectrics based absorbing layers, J. Appl. Phys. **116**, 043520 (2014).

[111] C. R. Simovski, M. Kondratiev, and S. He, An explicit method for calculating the reflection from an

anti-reflection structure involving array of C-shaped wire elements, J. Electromagn. Waves Appl. **14**, 1335 (2000).

[112] C. R. Simovski, M. Kondratiev, and S. He, Array of C-shaped wire elements for the reduction of reflection from a conducting plane, Microwave Opt. Technol. Lett. **25**, 302 (2000).

[113] M. Pu, C. Hu, M. Wang, C. Huang, Z. Zhao, C. Wang, Q. Feng, and X. Luo, Design principles for infrared wide-angle perfect absorber based on plasmonic structure, Opt. Express **19**, 17413 (2011).

[114] N. Liu, H. Guo, L. Fu, S. Kaiser, H. Schweizer, and H. Giessen, Plasmon hybridization in stacked cut-wire metamaterials, Adv. Mater. **19**, 3628 (2007).

[115] J. Dai, F. Ye, Y. Chen, M. Muhammed, M. Qiu, and M. Yan, Light absorber based on nano-spheres on a substrate reflector, Opt. Express **21**, 6697 (2013).

[116] S. A. Schelkunoff, The electromagnetic theory of coaxial transmission lines and cylindrical shields, Bell Syst. Tech. J. **13**, 532 (1934).

[117] J. McVay, A. Hoorfar, and N. Engheta, Thin absorbers using space-filling curve artificial magnetic conductors, Microwave Opt. Technol. Lett. **51**, 785 (2009).

[118] F. Bilotti, L. Nucci, and L. Vegni, An SRR based microwave absorber, Microwave Opt. Technol. Lett. **48**, 2171 (2006).

[119] Sukosin Thongrattanasiri, Frank H. L. Koppens, and F. Javier Garcia de Abajo, Complete Optical Absorption in Periodically Patterned Graphene, Phys. Rev. Lett. **108**, 047401 (2012).

[120] R. Alaee, M. Farhat, C. Rockstuhl, and F. Lederer, A perfect absorber made of a graphene micro-ribbon metamaterial, Opt. Express **20**, 28017 (2012).

[121] G. W. Hansen, Dyadic Green's functions and guided surface waves for a surface conductivity model of graphene, J. Appl. Phys. **103**, 064302 (2008).

[122] Y. Zhang, Y. Feng, B. Zhu, J. Zhao, and T. Jiang, Graphene based tunable metamaterial absorber and polarization modulation in terahertz frequency, Opt. Express **22**, 22743 (2014).

[123] A. Fernandez and A. Valenzuela, General solution for single-layer electromagnetic-wave absorber, Electron. Lett. **21**, 20 (1985).

[124] M. A. Kats, R. Blanchard, P. Genevet, and F. Capasso, Nanometre optical coatings based on strong interference effects in highly absorbing media, Nat. Mater. **12**, 20 (2013).

[125] J. Park, J.-H. Kang, A. P. Vasudev, D. T. Schoen, H. Kim, E. Hasman, and M. L. Brongersma, Omnidirectional near-unity absorption in an ultrathin planar semiconductor layer on a metal substrate, ACS Photonics **1**, 812 (2014).

[126] A. D. Rakić, A. B. Djurišić, J. M. Elazar, and M. L. Majewski, Optical properties of metallic films for vertical-cavity optoelectronic devices, Appl. Opt. **37**, 5271 (1998).

[127] A. Moreau, C. Ciracì, J. J. Mock, R. T. Hill, Q. Wang, B. J. Wiley, A. Chilkoti, and D. R. Smith, Controlled-reflectance surfaces with film-coupled colloidal nanoantennas, Nature (London) **492**, 86 (2012).

[128] M. Albooyeh and C. Simovski, Substrate-induced bianisotropy in plasmonic grids, J. Opt. **13**, 105102 (2011).

[129] M. Albooyeh, D. Morits, and C. R. Simovski, Electromagnetic characterization of substrated metasurfaces, Metamaterials **5**, 178 (2011).

[130] M. Albooyeh and C. R. Simovski, Huge local field enhancement in perfect plasmonic absorbers, Opt. Express **20**, 21888 (2012).

[131] J. Vehmas, Y. Ra'di, A. O. Karilainen, and S. A. Tretyakov, Eliminating electromagnetic scattering from small particles, IEEE Trans. Antennas Propag. **61**, 3747 (2013).

[132] M. Barbuto, A. Monti, F. Bilotti, and A. Toscano, in *Metamaterials 2011: Proceedings of the Fifth International Congress on Advanced Electromagnetic Materials in Microwaves and Optics, Barcelona, Spain, 2011* (Metamorphose VI, Brussels, Belgium, 2011), p. 86.

[133] Y. Ding and V. Fusco, Loading artificial magnetic conductor and artificial magnetic conductor absorber with negative impedance converter elements, Microwave Opt. Technol. Lett. **54**, 2111 (2012).

[134] K. L. Ford, in *Proceedings of the Antennas and Propagation Conference (LAPC), Loughborough, UK, 2013* (IEEE, New York, USA, 2013), p. 510.

[135] J. P. Turpin, J. A. Bossard, K. L. Morgan, D. H. Werner, and P. L. Werner, Reconfigurable and tunable metamaterials: A review of the theory and applications, Int. J. Antennas Propag. **2014**, 429837 (2014).

[136] I. S. Nefedov, C. A. Valagiannopoulos, S. M. Hashemi, and E. I. Nefedov, Total absorption in asymmetric hyperbolic media, Sci. Rep. **3**, 2662 (2013).

[137] M. Albooyeh, D. Morits, and S. Tretyakov, Effective electric and magnetic properties of metasurfaces in transition from crystalline to amorphous state, Phys. Rev. B **85**, 205110 (2012).

[138] *Amorphous Nanophotonics*, edited by C. Rockstuhl and T. Scharf (Springer, New York, 2013).

[139] J. D. Jackson, in *Classical Electrodynamics*, 3rd ed. (Wiley, New York, 1999).

[140] A. Kazemzadeh and A. Karlsson, On the absorption mechanism of ultra thin absorbers, IEEE Trans. Antennas Propag. **58**, 3310 (2010).